TAMPEREEN TEKNILLINEN YLIOPISTO
TAMPERE UNIVERSITY OF TECHNOLOGY

Effect of Adiabatic Heating on Strain Induced Phase Transformations in Stainless Steels

Ayat Soltani

Master of Science Thesis

TAMPERE UNIVERSITY OF TECHNOLOGY
(AUGUST 2013)

EXAMINERS: Professor Veli-Tapani Kuokkala,
Dr. Mikko Hokka, Dr. Matti Isakov

Abstract

TAMPERE UNIVERSITY OF TECHNOLOGY

Master of Science Major subject: Metallic materials

AYAT SOLTANI

Examiners: Professor Veli-Tapani Kuokkala, Dr. Mikko Hokka, Dr. Matti Isakov.

During plastic deformation, metastable austenitic stainless steels can go through a phase transformation from unstable austenite to martensite. This leads to an increase in the work hardening rate. Since steels are widely used metals, a lot of research efforts have been directed towards better understanding of their behavior. The phase transformation is one of the questions that have attracted a lot of attention from the researchers. This thesis focuses on studying the role of strain rate and adiabatic heating on the phase transformation from austenite to martensite during plastic deformation of metastable austenitic steels.

The materials used in this study were EN 1.4318 stainless steel and titanium Ti-6Al-4V alloy. Mechanical testing was carried out with a servohydraulic materials testing machine at strain rates ranging from 0.0003 s^{-1} to 1 s^{-1} and at heating rates ranging from 1.4K/min to 10K/min.

The results indicate that the strain induced phase transformation is affected by adiabatic heating but also by the strain rate itself. The results were obtained by measuring the temperature change during high strain rates and then applying the same heating rate to a lower strain rate test where test conditions without the heating would have been practically isothermal. The flow stress after 15% strain for the stainless steel at the strain rate of 0.03 s^{-1} was lower than the flow stress for the strain rate of 0.0003 s^{-1} with the continuous heating even though the temperature conditions for both strain rates were artificially kept similar throughout the test. Based on this observation it was concluded that the change in the strain rate had a noticeable effect on the flow stress. To confirm that this behavior was directly related to the phase transformation, similar tests were conducted for the titanium alloy, which does not go through any phase transformation during plastic deformation. The same heating rate that was measured during the deformation at the strain rate of 0.025 s^{-1} (none-isothermal deformation) was applied to the test that was performed at the strain rate of 0.0003 s^{-1} (isothermal deformation). The results showed that the flow stress for the strain rate of 0.0003 s^{-1} with continuous heating was lower than the flow stress for strain rate of 0.025 s^{-1} which was to be expected.

Preface

I would like to express my deepest gratitude to my teacher and supervisor Dr. Mikko Hokka. He inspired me to work hard during my studies at TUT and gave me this subject as my thesis to work on. He helped me immensely during the research and also his help and guidance during writing of this thesis proved to be very valuable. Without his help none of this would have been possible. I would like to thank Dr. Matti Isakov for taking time out of his busy schedule and walking me step by step and teaching me everything that I needed for this thesis. A big thanks to Professor Kuokkala for his help as well.

I also wish to thank my very good friend Ahmad Mardoukhi for his support and being there for me whenever I was down and wanted to talk to someone. Having someone such as him, who was working on his own thesis, proved to be very inspiring and enjoyable. I should also mention my friend Alireza Shahbazi, who spent so many hours drawing the plots and graphs that I could not draw myself.

Finally I would like to thank my then girlfriend and now wife, Niloofar, for being so supporting and patient with me during the past year. Her love was what kept me working hard.

August 2013

Ayat Soltani

Contents

Symbols and abbreviations

σ	Stress
E	Young's modulus
ε	Strain
$\dot{\varepsilon}$	Strain rate
W	Mechanical work done by plastic deformation
l_0	Initial length
l	Current length
F	Load
A_0	Initial cross section
ΔT	Change in temperature
ρ	Density
c_p	Heat capacity of the material
B	Taylor-Quinney coefficient
τ_{crss}	Critical shear stress for dislocation motion
σ^*	Thermal component of flow stress
σ_A	Athermal component of flow stress
σ_m	Maximum stress opposing the movement of dislocations
ε_0	Dimensionless material constant
P_t	Activation rate
P_b	Probability rate
V_g	Vibration frequency of the atoms
ΔG	Thermal energy
k	Boltzman`s constant

T	Temperature
Δt	Time that a dislocation takes to move between to obstacles
t_w	Waiting time
t_r	Run time
v_l	Frequency of successful surmounting attempt
M	Orientation factor
b	Burger`s vector
ΔG_0	Activation energy at 0 K
B	Viscous damping coefficient
FCC	Face centered cubic
BBC	Body centered cubic
BCT	Body center tetragonal
M_s	Start temperature of thermal martensite transformation
M_s^σ	Start temperature of stress-induced martensite transformation
M_d	Start temperature of strain-induced martensite transformation
σ_e	Engineering stress
ε_e	Engineering strain
σ_T	True stress
ε_T	True strain
A_i	Instantaneous cross section
l_i	Instantaneous gage length
$\dot{\varepsilon}_T$	True strain rate
Θ_T	True strain hardening rate

1 Introduction

Stainless steels are arguably one of the most widely used metal alloys today, especially in industries such as construction and petroleum. A good combination of low price, resistance to corrosion and high hardness has led to their widespread use, so it is not a surprise that different grades of stainless steels have been studied and research extensively in order to fully take advantage of their properties. One of the more complicated stainless steel grades are metastable austenitic stainless steels. During deformation, the phase transformation from austenite to martensite is initiated which improves the hardness of these stainless steels. However, this phase transformation is highly dependent on strain rate. When strain rate increases the deformation will change from isothermal towards adiabatic conditions which increases the temperature of the material considerably. This temperature increase will in turn, suppress the phase transformation from austenite to martensite and lowers the hardness of the stainless steel.

It has been long known that the temperature increase during deformation effects the phase transformation from austenite to martensite. However, not much effort has been directed towards separating the effects of strain rate from the effects of temperature increase. This thesis aimed to achieve this goal. By measuring the temperature increase during high strain deformation (non-isothermal) and applying it to low strain deformation (isothermal), the temperature during each stage of the deformation was the same for both strain rates. By comparing the stress-strain behavior and strain hardening abilities of the material for both strain rates, the effect of strain rate on mechanical behavior of the material during deformation was studied. For comparison, a metal which does not go through any phase transformation during deformation was used.

EN 1.4318 stainless steel was used as a metastable austenitic steel and titanium Ti-6Al-4V alloy, as the metal which does not go through any phase transformation. Deformation was done in tension using an Instron 8800 servohydraulic materials testing machine. A custom built elevated temperature setup originally made by Isakov [1] was utilized in order to minimize the effect of heat conduction from the specimen to the surrounding environment.

2 Plasticity of steels and phase transformation plastic during deformation

In this chapter plastic deformation and phase transformation during deformation of steels are discussed.

2.1 Elastic behavior of metals

The schematics for compressive and tensile deformations are shown in Figure 1(a) and (b), respectively. These Figures show how the geometry of the specimen changes during tension and compression.

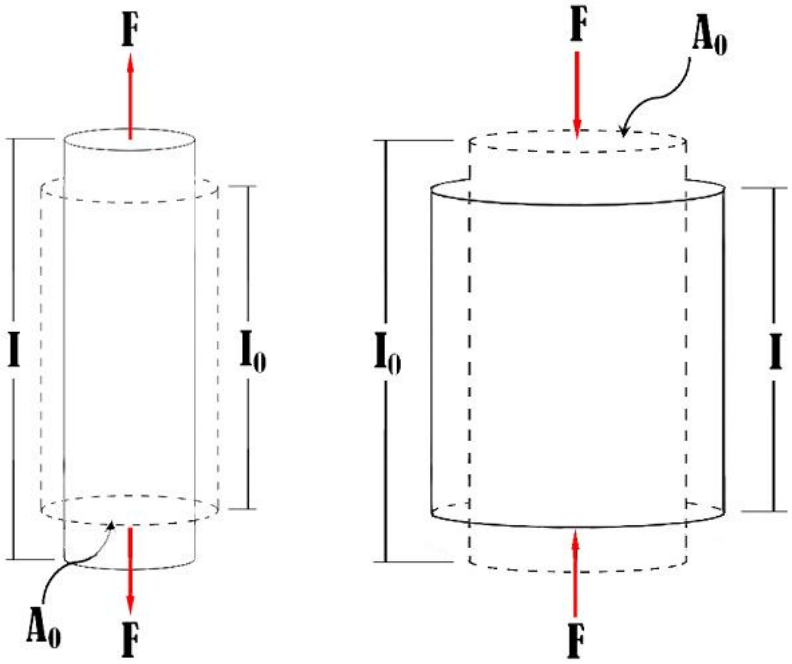

Figure 1. Schematic picture of tensile and compressive straining. l_0 is the initial length of the specimen, l length after deformation, F is the external load, and A_0 the initial cross section of the specimen.

When the metal is deformed at relatively low load levels the deformation is not permanent, and when the load is released the changes in the shape of the specimen return back to original. This behavior is observed in the elastic region of the stress-strain curve. The relationship for most metals between stress and strain is linear, as shown by Equation (2.1), where **E** is the modulus of elasticity or Young`s modulus. The elastic part of a schematic stress vs. strain curve is shown in Figure 2.

$$\sigma = E\varepsilon \tag{2.1}$$

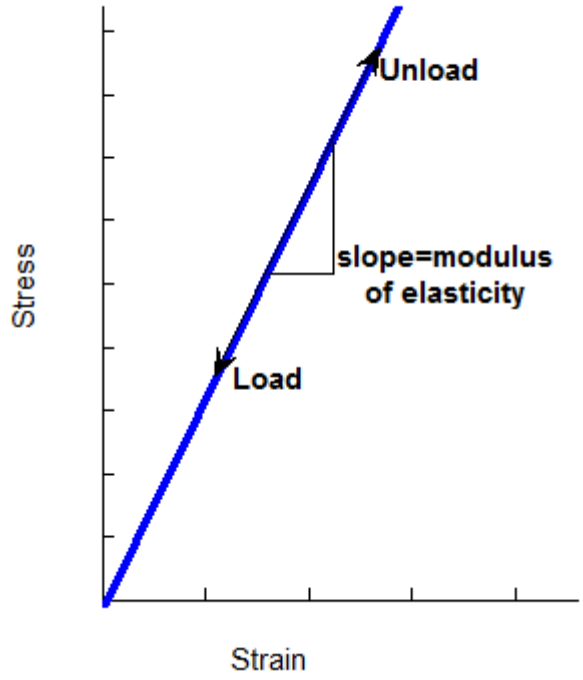

Figure 2. Elastic part of the stress-strain curve.

2.2 Plastic behavior of metals

When the stress reaches the yield point of the material, most of any further deformation is permanent, and if the load is removed the changes in the geometry are not fully recovered. As shown in Figure 3, the relationship between stress and strain is, at least in most cases, no longer linear. There are, however, exceptions, such as some TWIP (twinning induced plasticity) steels and certain nickel based superalloys, where the relationship is rather linear, but the slope of the plastic part is clearly different from that of the elastic part.

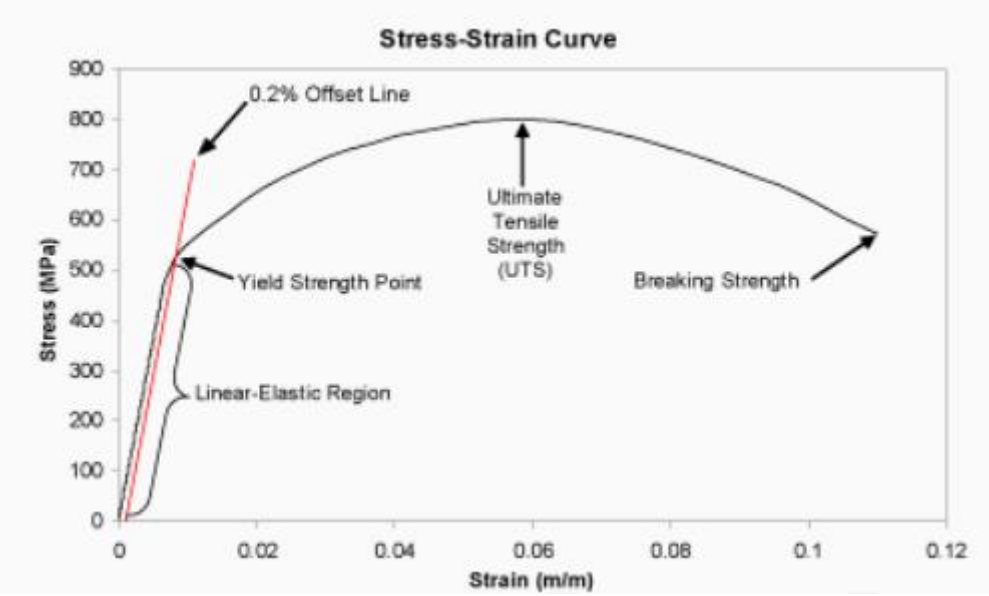

Figure 3. A typical stress-strain curve for steels showing both elastic and plastic regions [2].

The point at which the plastic region begins is called the yield point. The offset method can be used for calculating the yield point, since in most cases the yield point is not well defined and the upper part of the elastic region is not perfectly linear. The offset method involves plotting a line parallel to the elastic region starting from 0.2% strain and determining the yield point from the intersection of this line and the stress strain curve.

The point at which the deformation localizes is called the ultimate tensile strength. After this point the engineering stress decreases with strain since the cross sectional area decreases too fast and the strain hardening cannot compensate for the change in the geometry of the specimen.

Strain rate (usually indicated by $\dot{\varepsilon}$ as shown in Equation (2.2)) is the rate of change in the strain or in other words, deformation of the material with respect to time.

$$\dot{\varepsilon}=\frac{d\varepsilon}{dl} \tag{2.2}$$

2.3 Temperature change during deformation

Plastic deformation consumes mechanical energy that is brought to the material by the external force. However, considering the conservation of the energy, the total amount of energy used for the plastic deformation should only change into other forms of energy to keep the total amount of energy constant. The energy imported to the material will be either spent in the internal structures or it will simply convert to thermal energy. The thermal energy can increase the temperature of the material if the deformation is fast enough and the heat doesn't have time to be dissipated into the material's surroundings. However, experiments have shown that most of the energy consumed in the plastic deformation is transformed into heat. Only a small part is actually stored in the structure. This small part is estimated to be somewhere between 5-10 %, although it is highly dependent on the material in question (it can go as high as 60% in the case of 2024-T3 Al alloy at low levels of plastic strains, for example [3]). The remaining energy can lead to a temperature increase of tens of degrees in the material. If the deformation is concentrated in a small section, the temperature increase can even reach the melting point.

The time available for the generated heat to transfer away from the material is highly dependent on the strain rate. Low strain rates will lead to isothermal conditions whereas high strain rates will be more or less adiabatic. When the strain rate during the plastic deformation is low, the heat generated in the metal has enough time to transfer to the atmosphere surrounding the specimen or to a non-deforming part of the specimen. For most metals, such strain rate is typically around 10^{-1} [4]. The deformation blow these strain rates is isothermal, during which the temperature of the material remains constant. [5, 6] .

In practice, however, the change from fully isothermal conditions to fully adiabatic happens gradually. The region where this gradual change occurs is usually called quasi-isothermal or quasi-adiabatic. Under these conditions the thermal energy produced by plastic work only partially escapes to the material's surroundings and the temperature of the material increases, but not so strongly as in fully adiabatic conditions.

At high strain rates, the deformation is fast enough so that the heat does not have enough time to dissipate to the surrounding environment. At these conditions the heat transfer is

very low and can be disregarded, and the excess heat will increase the temperature of the metal.

The adiabatic heating can be estimated based on the work done by the plastic deformation. The work can be calculated using Equation (2.3):

$$W=\int_{l_0}^{l} f\ dl \qquad (2.3)$$

Where f is the load, l_0 is the initial length and l the current length after deformation. This Equation can be re-written as:

$$W=A_0\, l_0 \int^{\varepsilon} \sigma\,(\varepsilon) d\varepsilon \qquad (2.4)$$

Where A_0 and l_0 are the initial cross section and initial length of the specimen, respectively. If the heat stays in the specimen, the increase in temperature is given by:

$$\Delta T = \frac{\beta}{\rho c_p} \int^{\varepsilon} \sigma(d\varepsilon) \qquad (2.5)$$

In Equation (2.5), ρ is the density, c_p the heat capacity of the material, and β is the Taylor-Quinney coefficient, which tells how much of the total energy is converted to heat (usually β is between 0.5 and 0.9). The assumption here is that during the deformation the pressure is constant.

For example a temperature increase of 35 ^{0}C has been observed in tension testing of plain carbon steels at the strain rate of 8 x $10^{-2}\ s^{-1}$. The temperature increase can be as high as 55 ^{0}C at higher strain rates [5].

2.4 Plastic deformation by dislocation motion

When a crystalline metal is deformed, the deformation is carried out by the movement of structural defects called dislocations. When a dislocation moves through the crystal and reacts with other dislocations, it changes the overall energy of the structure. This usually means an increase in the total energy.

Various flaws and defects in the crystal act as obstacles for the moving dislocations. These obstacles can be thought as being any sort of variations in the overall energy of the crystal. The obstacles that hinder the movement of dislocations can be divided into two main categories: 1) long range obstacles, such as dislocation pile ups, and 2) short range obstacles, such as lattice defects, alloy atoms, vacancies, or interstitials.

If the resistance to the dislocation motion is τ_{crss}, the acting normal stress σ has to result in a higher resolved shear stress than τ_{crss} for the dislocations to move. If the external stress results in a lower resolved shear stress than τ_{crss}, additional energy is required for the dislocation movement. This excess energy can be acquired from thermal energy. The thermal energy of the crystal can facilitate the dislocation movement by helping the dislocations to surmount obstacles. This process is called thermally activated dislocation motion and it depends on time, and consequently, on the strain rate. If the energy required for dislocations to overcome an obstacle is very high, the thermal energy cannot assist the dislocation in surmounting the obstacle. In this case the energy needed for dislocation motion has to come entirely from external sources and the obstacles are called athermal [7, 8].

Based on the conclusion above, the flow stress comprises two parts: thermal (σ^*) and athermal (σ_A) stress.

$$\sigma = \sigma^* + \sigma_A \qquad (2.6)$$

The relationship between the stress and temperature at various strain rates is presented in Figure 4.

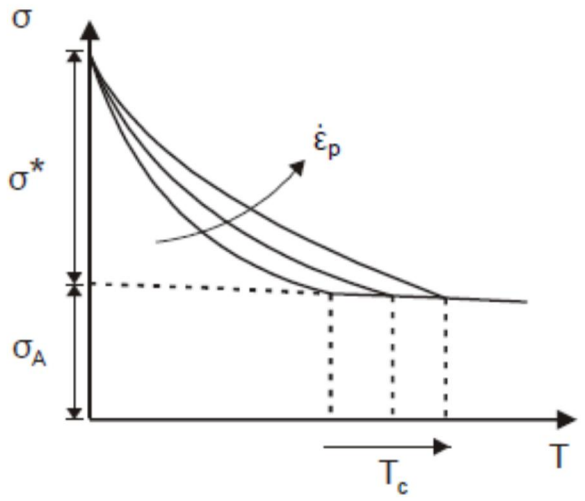

Figure 4. Dependence of flow stress (σ) on temperature (T) and strain rate (ε̇) [9].

If the temperature is increased above T_c, the deformation becomes essentially independent of temperature. At this critical temperature, enough thermal energy is available and all the short range obstacles are readily overcome without delay, and the flow stress consists of the athermal component only.

Figure 5 illustrates the Peierls stress as an example of the thermal obstacles. For these barriers there is a maximum force σ_m, which opposes the movement of dislocations. The stress driving the dislocation forward has to be more than the stress opposing the motion (σ_m) in order for the dislocation to overcome the barrier and to move on. With increasing temperature the amount of available thermal energy (ΔG) for overcoming obstacles increases. This is shown as hatched areas for different temperatures in Figure 6. In other words, as the temperature and consequently thermal energy increases, the amount of the required external energy or stress decreases.

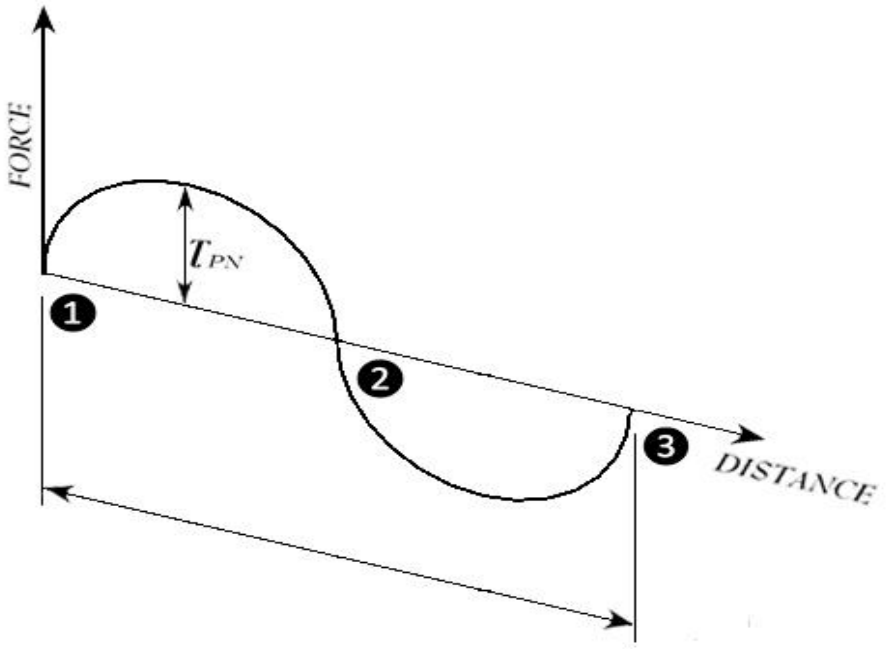

Figure 5. Distribution of force needed for overcoming Peierls forces. Modified from [9]

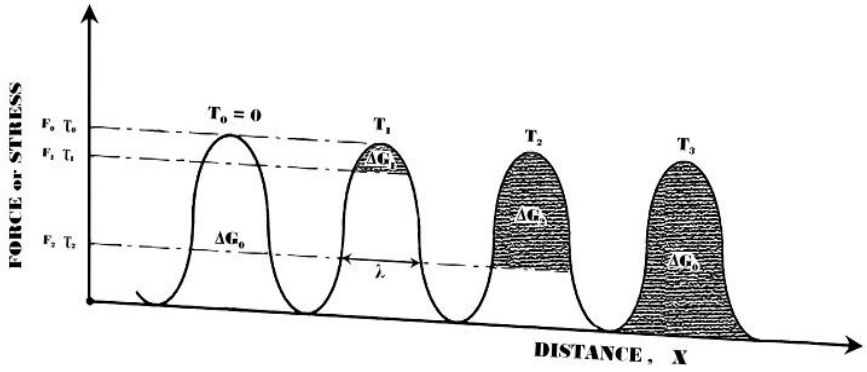

Figure 6. Thermal energy (ΔG) required for surmounting obstacles at different temperatures and stress σ. Modified from [9]

Figure 7 shows the stress vs. temperature plot based on the concept shown in Figure 6. [9].

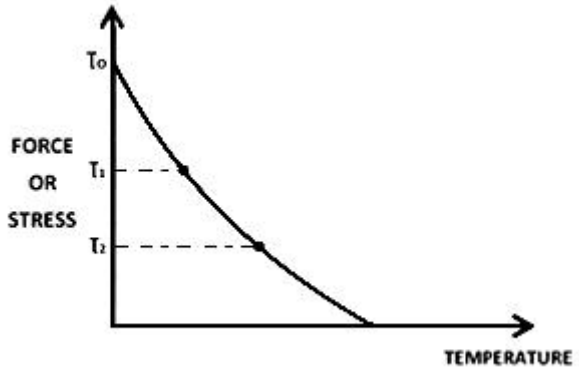

Figure 7. Strength of the material as a function of temperature [9].

The strain rate ε̇ can be expressed as:

$$\dot{\varepsilon} = \varepsilon_0 . P_t \qquad (2.7)$$

In this Equation ε_0 is a dimensionless material constant and P_t is the activation rate.

P_t represents the statistical nature of the thermal energy. It combines the frequency of the attempts to surmount the obstacle and the probability of these attempts being successful. The probability P_b of having a momentary energy greater than the critical ΔG is shown in Equation (2.8):

$$P_b = \exp(\frac{-\Delta G}{kT}) \qquad (2.8)$$

If V_g is the vibration frequency of the atoms, then activation rate can be expressed by:

$$P_t = v_g . P_b = v_g \exp(\frac{-\Delta G}{kT}) \qquad (2.9)$$

The time in which a dislocation moves between two obstacles can be divided to the waiting time in front of an obstacle t_w and the time when it runs between two consecutive obstacles t_r.

$$\Delta t = t_w + t_r \qquad (2.10)$$

If the frequency of successful attempts of surmounting of obstacles is given by v_l, which has the same value as (2.9):

$$v_l = v_g \exp\left(\frac{-\Delta G}{kT}\right) \tag{2.11}$$

Then the waiting time in front of the obstacle is calculated by:

$$t_w = \frac{1}{v_g \exp\left(\frac{-\Delta G}{kT}\right).} \tag{2.12}$$

The strain rate ε̇ can be expressed as (for details refer to [9]):

$$\frac{d\varepsilon}{dt} = \frac{1}{M}\rho b v \tag{2.13}$$

Where M is the orientation factor, ρ is the dislocation density, b is the Burgers vector, and v is the dislocation velocity. The velocity can be calculated by dividing the distance that the dislocation has moved by the time it takes to move that far, i.e.,

$$\frac{d\varepsilon}{dt} = \frac{1}{M}\rho b \frac{\Delta l}{\Delta t} \tag{2.14}$$

By discarding the running time in Equation (2.10) because the movement of dislocations is very fast and thus $t_w \gg t_r$, and using Equations (2.14) and (2.12):

$$\dot{\varepsilon} = \frac{v_g \rho b \Delta l}{M} \exp\left(\frac{-\Delta G}{kT}\right) \tag{2.15}$$

This can be simplified to:

$$\dot{\varepsilon} = \dot{\varepsilon}_0 \exp\left(\frac{-\Delta G}{kT}\right) \tag{2.16}$$

By taking ΔG as the total energy required for overcoming obstacles as the main variable,

$$\Delta G = kT ln \frac{\dot{\varepsilon}_0}{\dot{\varepsilon}} \tag{2.17}$$

This further clarifies what was presented in Figure 6. It was already shown that ΔG increases with increasing temperature, and Equation (2.17) shows how ΔG is related to temperature and strain rate.

By considering Figure 6 again and the fact that the hatched area represents ΔG, while keeping in mind that above T_c the flow stress is independent of temperature:

$$\Delta G \quad = \Delta G_0 - \int_0^{F^*} \lambda(f) dF \qquad (2.18)$$

Where the ΔG_0 is the activation energy at 0 K and the integral shows the non-hatched area. (λf i.e. work done by external stress) shows the barrier width. By using (2.17) and (2.18) one can deduce that:

$$kT ln \frac{\varepsilon_0}{\dot{\varepsilon}} = \Delta G_0 - \int_0^{F^*} \lambda(f) dF \qquad (2.19)$$

To summarize, as the temperature is increased the amount of energy for overcoming obstacles is increased (increase in the hatched area in Figure 6). At the same time larger obstacles can be surmounted at the same strain rate.

2.5 Strain induced phase transformations

A dislocation is called perfect when during glide the atoms above and below the glide plane are shifted by a distance, which is equal to the spacing of lattice points in the slip direction. The length of the Burgers vector of a perfect dislocation is equal to the distance between two adjacent lattice points. Figure 8 shows the lattice points and the Burgers vector of a perfect dislocation BB'.

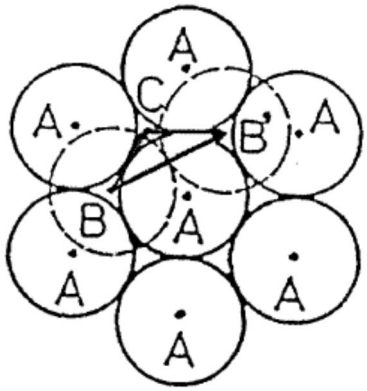

Figure 8. A schematic picture of the disassociation of a perfect dislocation BB' into two partial dislocations BC and CB' [8].

Each dislocation has a certain amount of elastic strain energy stored in it, and the energy is proportional to the square of its Burgers vector. So in some cases it is energetically

favorable for the dislocation to disassociate into two smaller dislocations, called partial dislocations. This dissociation is presented in Figure 8, as the deformation between B to B' can also be produced by deformation B to C and C to B'. This dissociation will change the stacking sequence of the lattice. The faulted stacking sequence is called a stacking fault. The width of the stacking fault depends on the amount of energy needed to generate the stacking fault, which is in turn related to the material in question. If the stacking fault energy is high, its width is relatively short and vice versa.

Alloying can affect the stacking fault energy of metals in a significant way [10]. For example according to various sources, the addition of Ni in stainless steels with less than 20% Cr significantly increases the stacking fault energy [11, 12, 13]. Stacking fault energy decreases when copper is alloyed with zinc or aluminum although the rate of decrease is higher in the case of aluminum, since aluminum itself tends to increase the stacking fault energy [14]. What makes matters even more complicated is the dependence of the stacking fault energy on temperature as well. To take stainless steels as an example again, the stacking fault energy increases with increasing temperature [15, 16]. A lot of experimental and theoretical work has been carried out to determine how the stacking fault energy changes under different circumstances, but the complicated nature of the subject coupled with various variables affecting it make this endeavor very difficult. The concept of disassociating dislocations plays an important role in the martensitic transformation, which will be covered next.

These days it is a very well-known fact that the austenite to martensite transformation initiates upon rapid cooling (or in other words quenching). When cooling rates are high, carbon atoms do not have enough time to diffuse out of the structure so they become trapped. The structure changes from FCC to BCT to accommodate the excess carbon atoms.

The transformation from ϒ-austenite to α' -martensite is very fast, and therefore, it is very difficult to study the details of this phase transformation. There are a few theories that have been introduced in the past to explain this phenomenon. Some have suggested that dislocations may assist the transformation by disassociation of the dislocation to Shockleys under straining [17]:

$$\frac{a}{2}[\bar{1}10] = \frac{a}{6}[\bar{2}11] + \frac{a}{6}[\bar{1}2\bar{1}] \qquad (2.20)$$

The atoms need to move half the length of these Shockleys in order to generate the BCT structure. This however in itself is not enough, so it has been proposed by Cina [18] and Mangonon et al. [19] that an intermediate phase transformation is required.

$$\text{ϒ} \dashrightarrow \varepsilon' \dashrightarrow \alpha' \qquad (2.21)$$

Here, ε' is a hexagonal structure, which then transforms to BCT α'. A more detailed review of this phenomenon is presented in Chapter 2.4.3.

According to Olson and Cohen [16], the strain-induced martensitic transformation is initiated in a discrete temperature range, as presented in Figure 9.

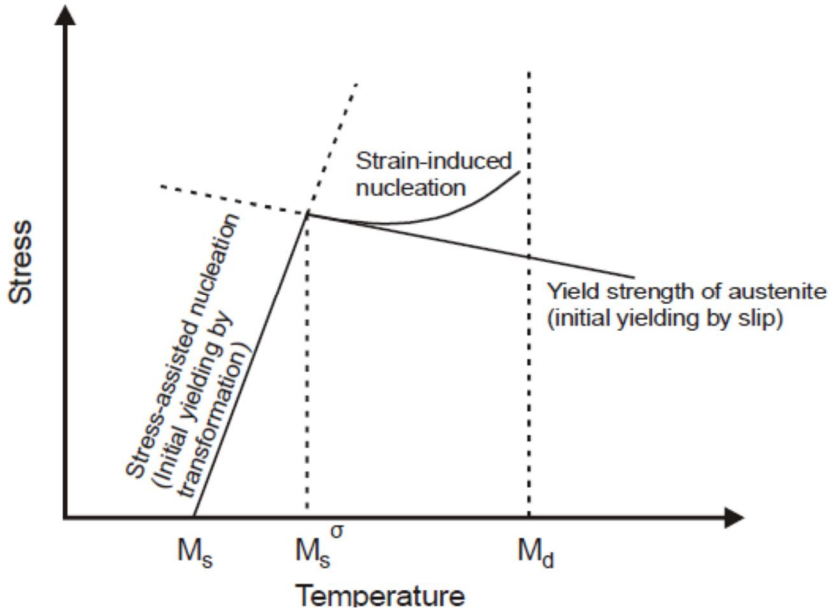

Figure 9. Martensite formation at different temperatures and stress levels [20].

If the temperature is reduced below the M_s temperature, the transformation from austenite to martensite happens spontaneously without any external force. The reason is that at these temperatures the chemical driving force is high enough. At temperatures below M_s^σ and above M_s, martensitic transformation is initiated below the yield stress while being assisted by external stresses. The stress required for the nucleation of martensite increases with increasing temperatures, because the chemical driving energy for the phase transformation decreases. Above M_s^σ, the external stress needs to reach or exceed the yield point of the austenite for the martensite transformation to start.

At temperatures above M_s^σ the stress, at which the transformation to martensite is initiated, is much lower than the stress assisted line extrapolated from below M_s^σ(the dashed line); this indicates that another mechanism for nucleation should be at work in this region. As the deformation proceeds further, the number of potential nucleation sites increases and the stress required for further nucleation decreases. This is the region, in which the strain directly affects martensitic transformation, hence the name strain-induced transformation.

2.5.1 Formation of ε martensite

Stacking faults are formed when the dissociation, such as the one presented in Equation (2.21), is initiated. These stacking faults will change the stacking sequence of {111} planes from the normal FCC stacking sequence {…ABCABCABC…} to {…ABC*ACA*BCA…}. These kind of stacking faults are called intrinsic stacking faults. Now let's consider a situation where two intrinsic stacking faults lay on consecutive {111} planes. In this case, the sequence of the planes will change to ABCACBCAB. This is called an extrinsic stacking fault.

A sequence of thin CAC and CBC layers is formed as a result of the change in the stacking sequence of the {111} planes. The structures of these layers are that of a closed-packed hexagonal and they can act as a nucleus for the HCP martensite formation [21]. Since the continued growth of the ε martensite is initiated by consequent stacking of the stacking faults at every second {111} plane [21, 10], it is hard to detect the differences between single stacking faults, bundles of overlapping stacking faults, and ε martensite.

According to Brooks et al. [21] and Venables [10] , the orientation relationship between the austenite and the two forms of martensite are as follows:

$$\Upsilon\ \{1111\}\ \text{II}\ \ \varepsilon\{0001\}\ \text{II}\ \alpha'\ \{101\} \tag{2.22}$$

$$\Upsilon\langle 110\rangle\ \text{II}\ \varepsilon\ \langle 1\bar{1}20\rangle\ \text{II}\ \alpha'\langle \bar{1}\bar{1}\bar{1}\rangle$$

Overall it has not been an easy task to clearly define the details of the ε martensite formation. Previous research [22, 18, 23, 19] indicates that some authors have postulated that the ε-martensite acts as an intermediate phase for α' martensite, which is covered in the next section. When studying the plastic deformation of AISI 304 steel at low temperatures, Gunther et al. and Mongonon et al. [19, 24, 25] found considerable amounts of ε to be present. Conversely Narutani [26] and Olson et al. [27] did not find any ε when the experiment was conducted under similar conditions.

2.5.2 Formation of α' martensite

The crystal structure of the α' martensite is BCT, and it can be formed when shear bands intersect with one another [10, 21, 19, 24, 28]. Lee et al. [29] and Grey et al. [30] have found that the nucleation of α' can also happen within a single shear band.

According to Olson and Cohen [16], the α' martensite is formed by two shears of the original FCC structure. First one is the 1/3 FCC twining shear of austenite and the second is the 1/2 FCC twining shear, which are referred to as T/3 and T/2, respectively. T/3 shear is possible by spreading an array of a/6<112> Shockley partials on every third {111} plane, and t/2 by spreading of Shockely partials on every second {111}. Shockley partials on every second {111} result in a perfect ε martensite. On this basis, it was suggested by Olson and Cohen that the α' nucleation is facilitated when the T/3 shears through ε martensite platelet.

It should be noted, however, that the formation of α' martensite is highly dependent on the stacking fault energy. While low SFE promotes the formation of shear bands and deformation twins, high SFE will act in an opposite manner resulting in a decrease in the nucleation of α' martensite. If a Shockley partial dislocation that is gliding on an austenite $(1\bar{1}\bar{1})$ plane crosses a deformation twin on the austenite (111) plane, the following dislocation reaction may happen [31] :

$$\frac{1}{6}[112] \rightarrow \frac{1}{6}[112]t + \frac{1}{9}[\bar{1}\bar{1}2]t \qquad (2.23)$$

Here t notes the Burgers vectors in the twin system. This reaction will lead to the nucleation of α' martensite with a BCC structure while continuing the plastic deformation. After the initial nucleation, the α' martensite grows by continued nucleation and coalescence of martensite embryos [32].

2.6 Effects of chemical composition, strain, stress, and grain size on the strain induced martensitic phase transformation

Chemical composition or alloying of the steel will have a strong effect on the martensite transformation. This is basically due to the fact that alloying affects strongly the SFE and the driving force for the transformation. One of the first equations that formulated the effect of alloying elements on strain induced martensite formation was presented by Angel [33]:

$$M_{d30}\ (^{\circ}\mathrm{C}) = 413 - 462\ (\%C + \%N) - 9.2\%Si - 8.1\%Mn - 13.7\%Cr - 9.5\%Ni - 18.5\%Mo \quad (2.24)$$

This Equation gives the temperature at which 50% of the structure is transformed to martensite at 0.3 strain based on the alloy composition.

According to Angel [33], the driving force for the martensite transformation decreases with increasing temperature. Figure 10 shows some of the work by Angel. It can clearly be seen that the amount of martensite decreases as the temperature is increased, relating to the decreasing driving force.

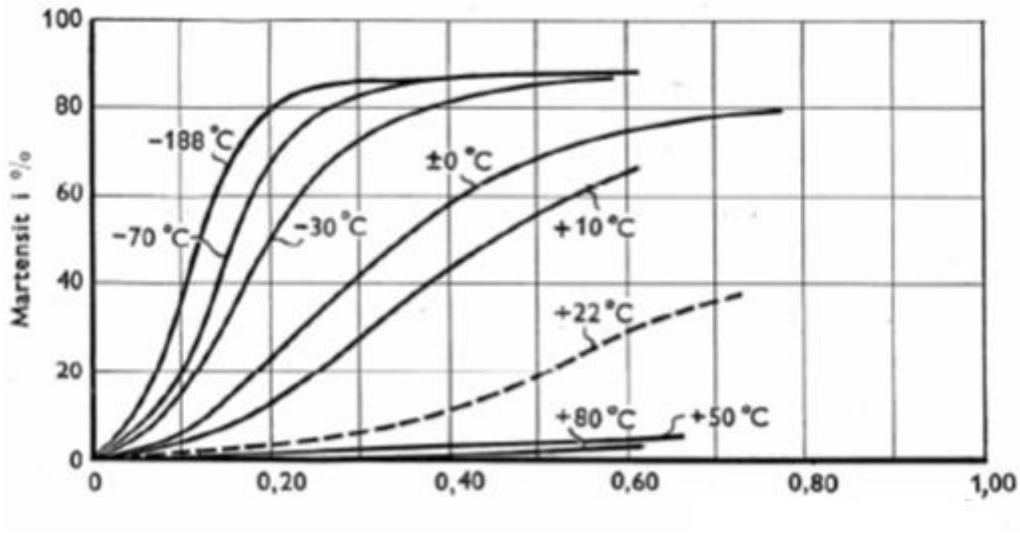

Figure 10. Effect of temperature on the strain induced martensite transformation during tensile deformation [33].

As discussed previously, higher strain rates will cause adiabatic heating, which can lower the amount of martensite by decreasing the driving force [32, 34, 35]. Apart from this, according to the discussion by Hecker et al. [35] and Murr et al. [32], the deformation at high strain rates can lead to the formation of shear-bands that can act as nucleation sites for the martensite, and thus enhance the martensite formation. However, this is true only for the early stages of deformation as shown in Figure 11. At strains lower than 0.25, the shear bands contribute to the formation of martensite, but at strains higher than this will induce adiabatic heating and consequently suppress the phase transformation.

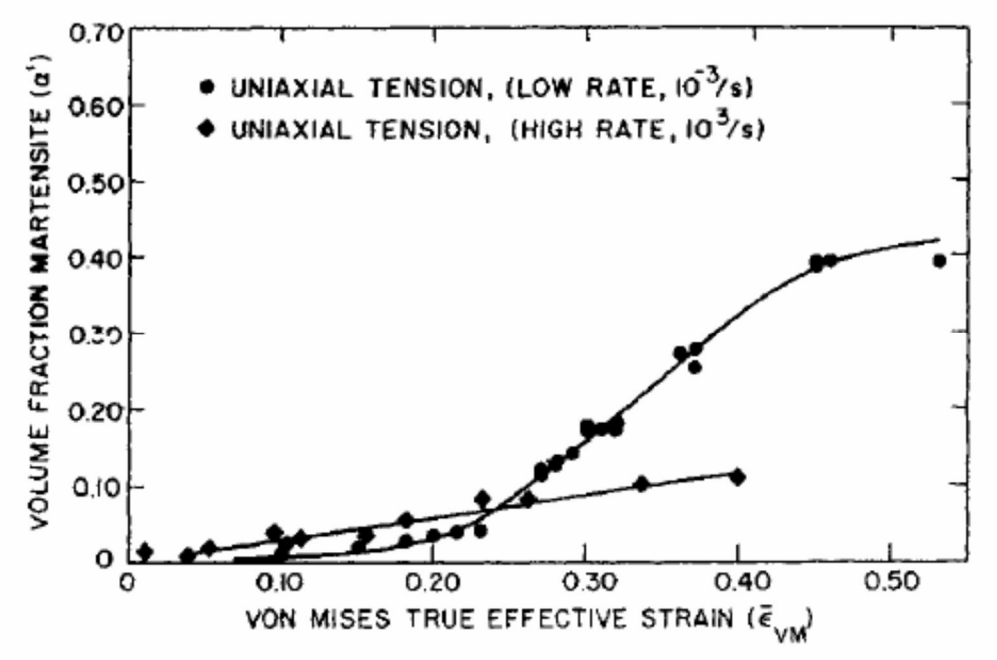

Figure 11. Effects of strain rate on the strain induced martensite transformation [35].

Effects of stress, on the other hand, have been extensively investigated in the past. According to Patel et al. [36] and Hecker et al. [35], biaxial stress state produces more martensite compared to the uniaxial state. Powel et al. [37] found that the martensite formation was faster in tension than in compression, and Murr et al. [32] explained that this was because of the larger amount of active shear bands available in biaxial tension than in compression.

According to Gonzales et al. [38] and Varma et al. [39], larger grain size will positively contribute to the formation of martensite during deformation. The results confirm the modification of (2.24):

$$M_{d30}\ (^{\circ}\mathrm{C}) = 551 - 462\ (\%C + \%N) - 9.2\%Si - 8.1\%Mn - 13.7\%Cr - 29(\%Ni + \%Cu) - 18.5\%Mo - 68\%Nb - 1.42(GS-8) \qquad (2.25)$$

Here the term GS is the ASTM grain size and it is obvious that the martensite formation temperature increases with increasing grain size.

2.7 Effects of strain induced α'-martensite on the mechanical properties

The studies by Huang et al. [40], Pineau et al. [31], and Byun et al. [41] have shown the already well-known fact that the formation of α'-martensite is accompanied by an increase in the work-hardening rate and hardness. Figure 12 shows the work-hardening rate as a function of strain at different temperatures.

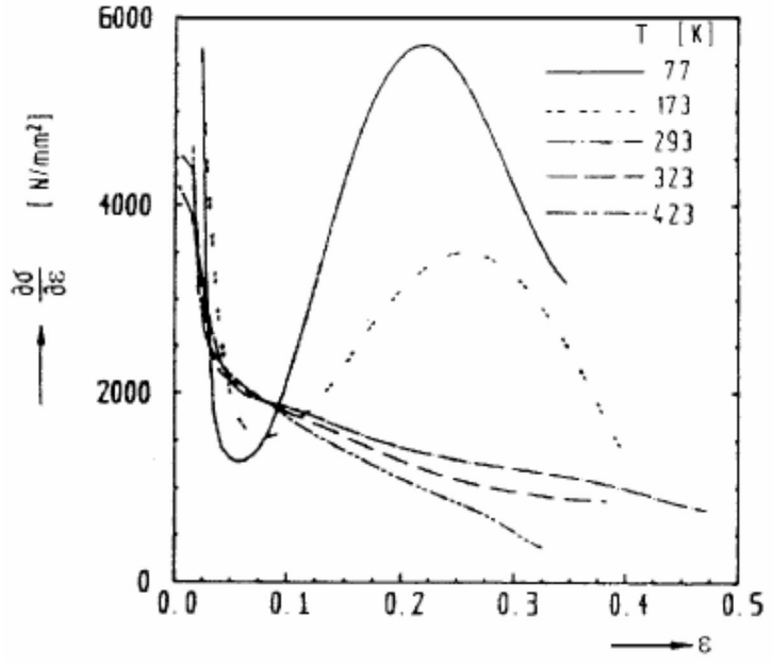

Figure 12. Work-hardening rate as a function of strain at different temperatures for AISI 304 steel [42].

The tests in Figure 12 were performed at temperatures where the phase transformation occurs as well as at temperatures where no transformations can occur. When looking at the curves obtained at two of the lowest temperatures, we observe a rapidly decreasing strain hardening rate at low strains, but at strains higher than about 7% of deformation the strain hardening rate increases rapidly, and a maximum value is achieved at strains of around 20-25%. This behavior is very different from that normally observed for metals and alloys, i.e. the work-hardening rate decreases with strain. The strong increase in the strain hardening rate has been attributed to the formation of the α'-martensite. Another interesting feature that can be deduced from Figure 12 is how the formation of the α'-martensite is highly temperature dependent, as the phase transformation is suppressed at higher temperatures.

The appearance of the minimum strain hardening rate at strains around 0.05 was related to the formation of the ε phase by De et al. [43] and Gunther et al. [24]. However, this theory was opposed by Suzuki et al. [28], who related this minimum to a reduction in the strain hardening at the start of α' formation. Later this effect, which was termed the dynamic softening effect, was explained by Narutani et al. [27] to originate from how α' formation acts as an additional deformation mechanism along with the normal dislocation slip. However, Fang et al. [42] mentioned only the volume change during deformation as the reason for this effect.

A clear maximum in the elongation values is often observed at certain temperatures for steels where strain induced phase transformations occur. An example of this is shown in Figure 13.

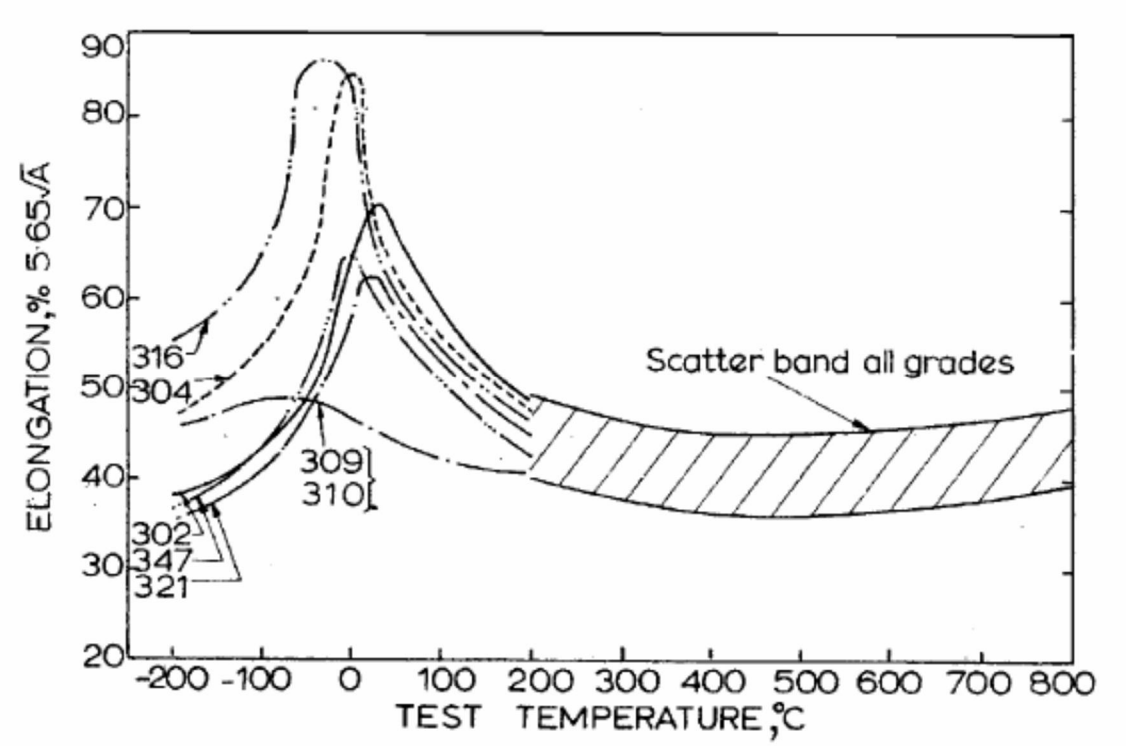

Figure 13. Elongation as a function of temperature [44].

This behavior has been explained by various researches [40, 41, 45], and it is related to the rate of α'-martensite formation. Since martensite is harder than the rest of the steel, its formation will prevent the plastic deformation from localizing. Therefore this enhances the ductility of the steel. As the temperature increases from the maximum elongation value, the transformation of austenite to martensite is slow, and the ductility is slowly reduced as the temperature is increased. At lower temperatures, however, this phase transformation is fast and it happens already at low strains, so the work hardening is very strong at low strains

and the phase transformation capability is exhausted too early resulting in fracture before considerable elongation. Somewhere between these two extremes there is a temperature range where the phase transformation proceeds gradually with strain, producing just enough martensite to prevent the strain localizations, leading to very high elongation values. A study by Bhadeshia [46] showed that when the austenite fully transforms to α'-martensite, the maximum tensile elongation due to this transformation is about 15%. However in TRIP steels, which were the subject of his studies, only 2% out of the total 15-30% of uniform tensile strain was the consequence of transformation plasticity. For this reason he argues that perhaps the role of TRIP was exaggerated in explaining the good properties of these steels.

One of the explanations for the strengthening mechanisms in metastable austenitic steels where the α'-martensite transformations occurs, was presented by Narutani et al. [27]. As explained in the previous sections, the flow stress is affected by the hardening effect of the α' formation and the dynamic softening effect when α'-martensite transformations acts as an alternative deformation mechanism. Mangonen and Thomas [19] observed a linear dependence between the yield strength and the fraction of α' martensite. They assumed that the steel shows a composite structure when the phase transformation from austenite to martensite occurs, comprising a hard martensite phase in a soft austenite matrix. Here the martensite acts as a reinforcing phase for the whole structure. The role of α'-martensite in the strengthening of the steel was further studied and verified by Guimarães and De Angelis [47] and Guimarães and Eckstein [48]. They concluded that martensite formation will decrease the effective grain size and increase the dislocation density in the austenite phase. They also concluded that the plastic deformation occurs in the austenite, while at the same time the martensite reduces the grain size of the austenite.

3 Experimental

The mechanical behavior of the studied material was characterized in tension at different temperatures. The tension tests were conducted at strain rates ranging from 0.0003 s^{-1} to 1 s^{-1}. At higher strain rates the adiabatic heating changes the specimen temperature, whereas at low strain rates the conditions are isothermal. The temperature change at the adiabatic conditions was calculated and this data was used to replicate similar heating rates in the low strain rate tests, which are normally isothermal. More details on how the tests were performed are given in Chapter 3.3.

3.1 Specimens

The materials studied in this work were austenitic stainless steel sheet EN 1.4318 (AISI 301LN)-2B and grade 5 Titanium alloy Ti-6Al-4V sheet. The thickness of the austenitic stainless steel and the titanium alloy were 2.0 mm and 1.0 mm, respectively. Figures 14-15 show the geometry and dimensions of the tension specimens used in the tests.

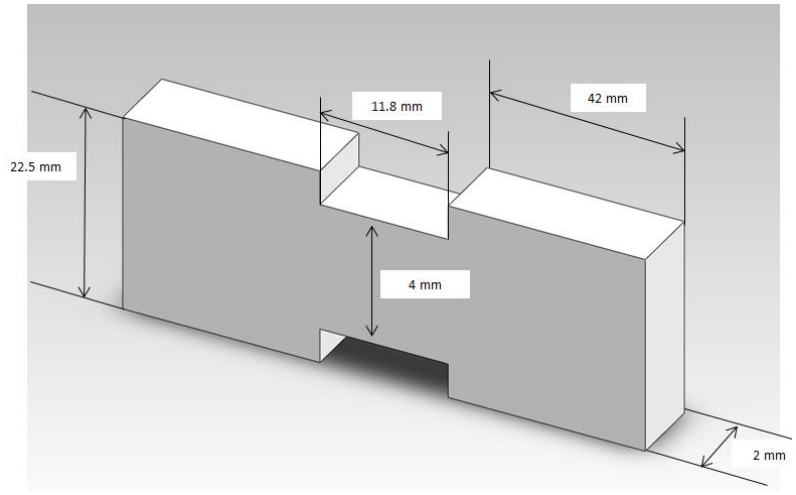

Figure 14. Specimen geometry for the stainless steel.

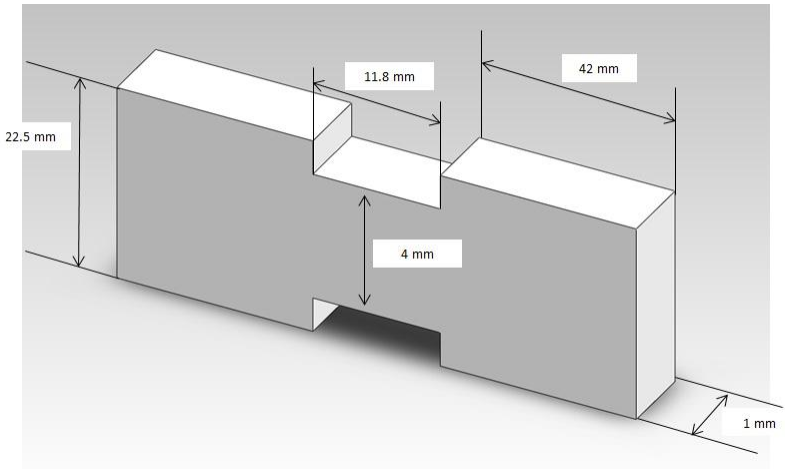

Figure 15. Specimen geometry for the titanium alloy.

3.2 Calculating stress and strain

Engineering stress and strain were calculated using:

$$\sigma_E = \frac{F}{A_0} \tag{3.1}$$

$$\varepsilon_E = \frac{\Delta l}{l_0} \tag{3.2}$$

Equation (3.1) is the engineering stress and Equation (3.2) is the engineering strain. F is the load exerted on the specimen, A_0 is the original cross section, and l_0 and Δl are the original length and the change in the length, respectively.

Strain rate was calculated using:

$$\dot{\varepsilon} = \frac{d\Delta l}{dt l_0} \tag{3.3}$$

In reality it is obvious that both the length and the cross section of the material change as the deformation continues, and that the true values of the stress and strain cannot be based on the initial values of cross section and length. For this reason it is desirable to calculate the so-called true stress and true strain, which are based on the length and area at each moment during the deformation.

$$\sigma_t = \frac{F}{A_i} = \sigma_e(1 + \varepsilon_e) \quad (3.4)$$

$$d\varepsilon_t = \frac{dl_i}{l} \rightarrow \varepsilon_T = \ln(1 + \varepsilon_e) \quad (3.5)$$

Here A_i and l_i are the current or instantaneous cross section and length of the specimen, respectively. It should be noted that these equations are valid only until the onset of necking, where the deformation localizes. Finally, true strain rate and true strain hardening rate are given by Equations 3.6 and 3.7:

$$\dot{\varepsilon}_t = \frac{d\varepsilon}{dt} \quad (3.6)$$

$$\Theta_t = \frac{d\sigma_T}{d\varepsilon_T} \quad (3.7)$$

The theoretical temperature increase during the experiments was calculated using Equation (2.5) given in the previous Chapter.

3.3 Test setup

The tension tests were done using an Instron 8800 servohydraulic materials testing machine. Load was measured using a 100kN load cell, and the strain was measured using a dynamic extensometer with a 6 mm gauge length. The specimen was fixed in the hydraulic wedges of the Instron machine, or they were secured by passing a bolt through the lower and upper parts of the specimen and tightened with nuts.

A custom built elevated temperature setup originally made by Isakov [1] was used for simulating the adiabatic heating process. Figure 16 shows a picture of the high temperature setup. The heating chamber was large enough to house both the heating elements and the extensometer without any contact neither with the Instron machine nor with the heating chamber itself.

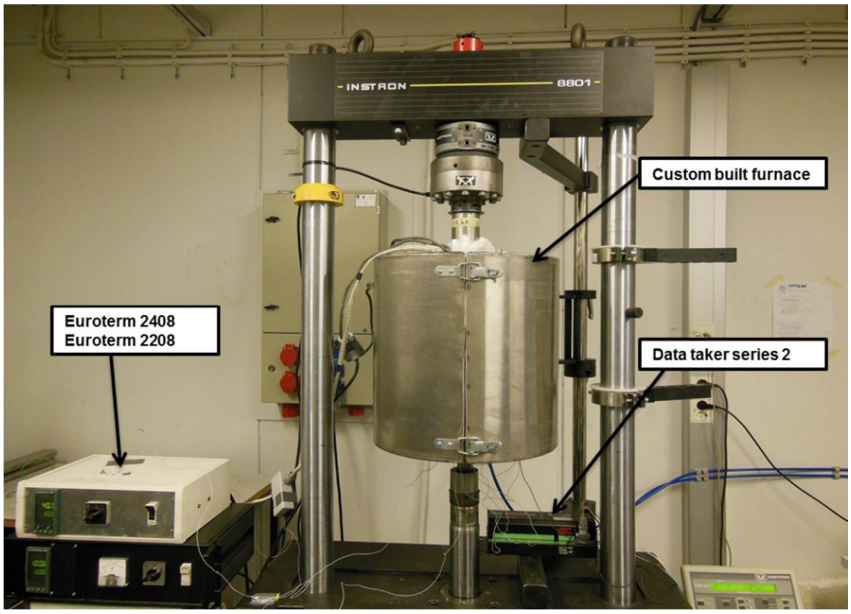

(a)

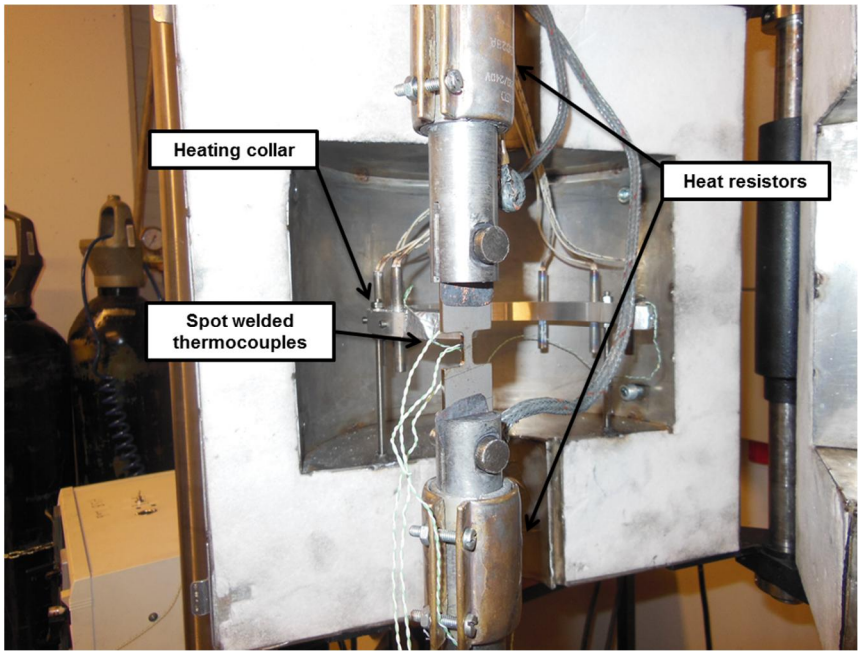

(b)

Figure 16. a)the custom built furnace attached to the Instron machine b) heat resistors and the aluminum collars.

The specimen was heated using a Euroterm 2408 PID controller, which controls the thyristor unit powering up the heating resistors. These resistors are attached to the upper and lower grips holding the specimen. To ensure that the temperature of the specimen is the

same inside the furnace and no heat transfer occurs, an aluminum collar was placed around the specimen. This collar was connected to another PID controller, Eurotherm 2208. Three K-type thermocouples were spot welded to the upper, middle, and lower parts of the specimen for in-situ measurement of the temperature the specimen length.

The tests were conducted at room temperature since the aim of this study was to replicate the temperature rise when the specimen is deformed at high strain rates. The strain rate for this test was chosen to be high enough to cause adiabatic heating in the specimen. The change in the temperature was calculated using Equations (2.5) which also give the temperature increase as a function of time. Using the main PID controller, this temperature increase was applied to another specimen loaded at significantly lower strain rate, where no or very little adiabatic heating occurs. In another test, the temperature increase during the same high strain rate was measured for comparison with the calculated values.

Replicating the exact temperature increase, however, proved to be quite challenging. The difference between the temperatures shown on the PID controllers was more than 5 C^0 and the difference increased as the temperature went higher. For this reason, the temperature shown on the PIDs was used only as a reference. During the first few seconds of loading, a temperature drop of about 5 C^0 was noticed in the specimen. Since the same drop in the temperature was measured for the aluminum collar, it was deduced that most probably interference from the test setup was causing disturbance in the thermo-couples.

A few tests were conducted in order to find out the correct temperature increase on the PIDs that result in the required heating rate in the specimen. It should be mentioned that since the thermal conductivity of the steel and the titanium alloy were different from each other, specific settings were needed for each of the materials.

4 Results and discussion

4.1 Stainless steel

Figure 17 shows the engineering and true stress vs. strain plots obtained at the strain rates of 0.0003 s^{-1} and 0.03 s^{-1} at room temperature.

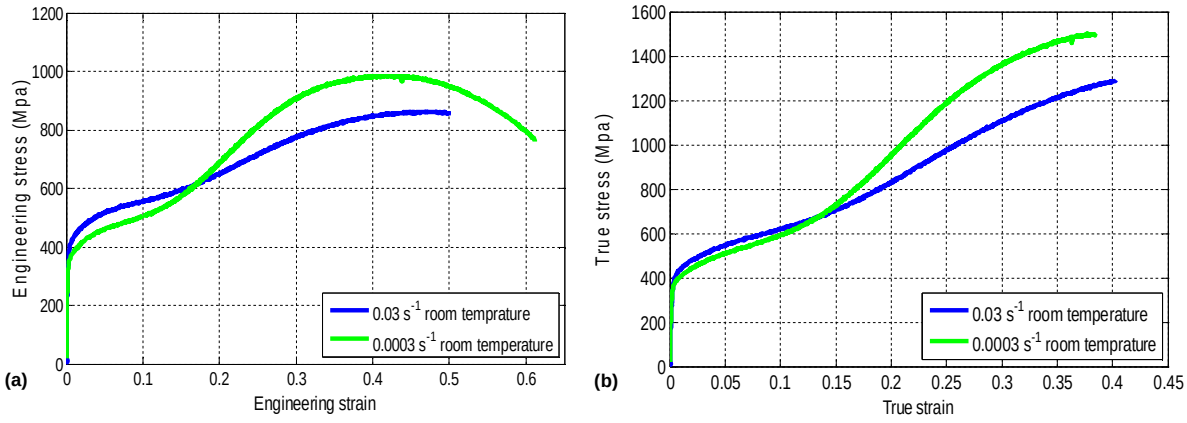

Figure 17. a) Engineering and b) true stress- strain curves for the stainless steel at strain

The most obvious difference between the stress-strain curves obtained at the two strain rates is the shape of the curves as it changes from sigmoidal towards parabolic upon an increase in the strain rate. This is especially clear in the case of the engineering stress-stain curve. The specimen tested at the strain rate of 0.0003 s^{-1} shows higher tensile strength compared to the tensile strength obtained at the strain rate of 0.03 s^{-1}. This behavior has been well documented for stainless steels in many publications [34, 49, 50, 1]. Another interesting feature is how the material behavior changes at around 0.15 of true strain. Before this point the flow stress in the test performed at the strain rate of 0.03 s^{-1} is higher than that of the material at 0.0003 s^{-1}. However, at strains higher than 0.15 the flow stress of the material at lower strain rate is higher. This phenomenon has been observed by Andrade et al. [51] and Lichtenfeld et al. [50]. Andrade et al. [51] conducted similar experiments, but with a more stable AISI 304 stainless steel, and noticed similar behavior at higher true strain rate than in the current experiment. The reason for this behavior is the change in the strain hardening rate at these two strain rates because phase transformation from austenite to martensite is happening at a different rate.

The reason for the change in the shape of the curves with increasing strain rate is the direct result of two opposite phenomena competing with each other; work hardening and thermal softening**.** Work hardening is related to the decreasing dislocation mobility during deformation, and it is stronger than the thermal softening at low strains, during which martensite formation will act as a strengthening mechanism and hinder necking [49].Thermal softening occurs when during deforming at higher strains the temperature of the specimen increases. This is particularly true in the case of stainless steels since their thermal conductivity is low, which results in a considerable increase in the temperature [52, 53, 54]. This phenomenon is dominant at higher strains leading to a reduction in the formed martensite and consequently, lower strength. Figure 18 shows the increase in the temperature measured with thermocouples for both strain rates used in this study. It clearly shows that the deformation at the strain rate of 0.03 s^{-1} increases the temperature of the material by more than 50 C^0. On the other hand, the deformation at the strain rate of 0.0003 s^{-1} does not essentially change the material temperature.

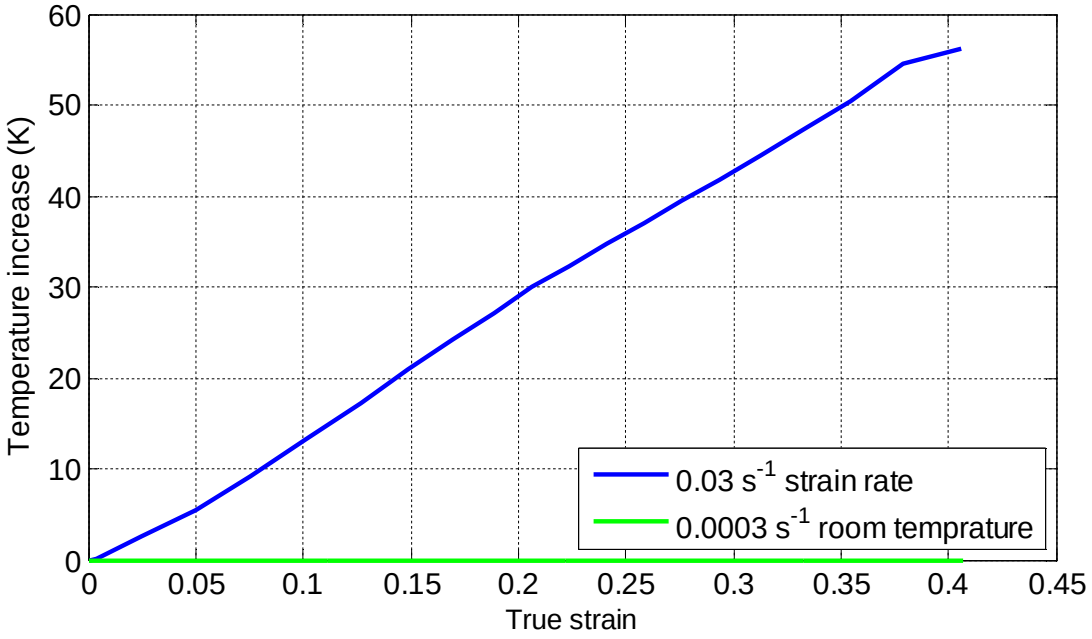

Figure 18. Adiabatic heating during deformation at the studied strain rates.

The change in the behavior of the material upon a change in the strain rate can be better understood by looking at the strain hardening rate as a function of true strain, as presented in Figure 19.

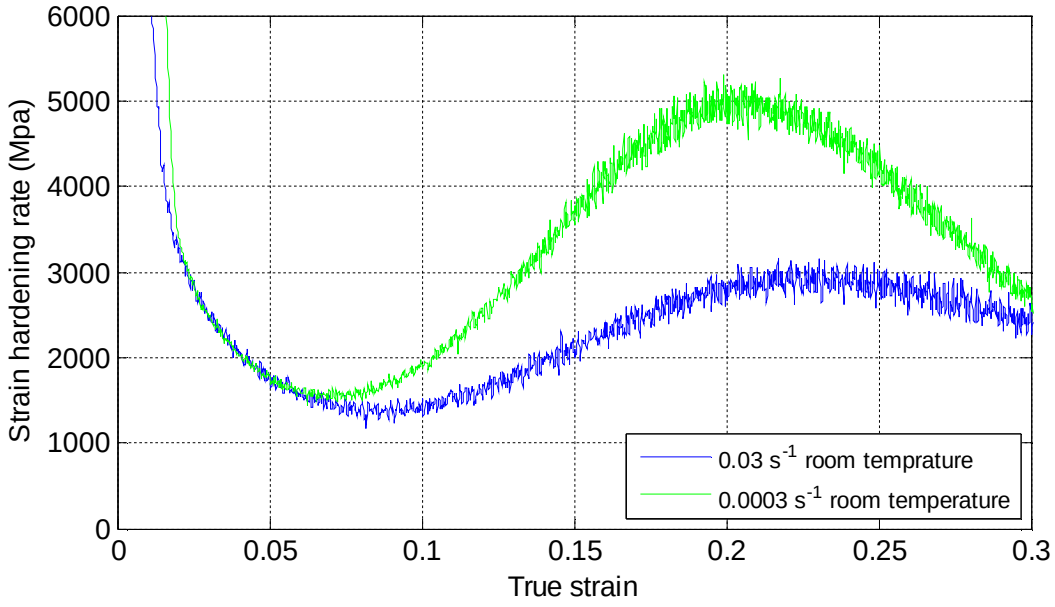

Figure 19. Effect strain rate on the strain hardening behavior.

Until 5% of true strain both curves follow the same path, but at strains higher than this the curves increasingly deviate from each other. The strain hardening at the strain rate of 0.0003 s^{-1} increases at a faster rate than at the strain rate of 0.03 s^{-1}, leading to a higher value of maximum strain hardening. This value is reached at a slightly lower true strain. This further clarifies how martensite formation during low strain rates will result in a stronger strain hardening compared to the strain hardening at higher strain rates. The curves presented here are also in accordance with other publications on similar steels and other metals. It has been a usual practice to divide the strain hardening curves into three stages to better understand the material`s behavior during deformation [43, 50, 55, 56, 57]. Stage 1, in which the strain hardening rate is rapidly decreasing at both strain rates is related to the onset of yielding. Before this point the deformation is elastic throughout the specimen. At the beginning of stage 2 (7% strain) strain hardening increases considerably, especially at lower strain rates. Here high stress exerted on the specimen will lead to increased dislocation mobility and velocity [43]. Stage 3 which begins at around 20% strain is where strain hardening rate decreases rapidly.

At the first stages of straining, especially at high strain rates, martensite formation will hinder local necking and increase the strain hardening rate [58]. However, further straining will weaken the effect of strain hardening as the heat retained in the material will increase the temperature and stabilize the austenite phase. This will lead to a reduction in the transformation rate and consequently a reduction in the strain hardening capability of the material.

Finally it is worth mentioning that unlike the initial assumption, circumstances during such tests are not always fully adiabatic. To demonstrate this, the increase in the temperature is calculated for the test performed at the strain rate of 0.03 s^{-1} using Equation (2.5). The calculated temperature and the measured temperature are plotted against true strain in Figure 20.

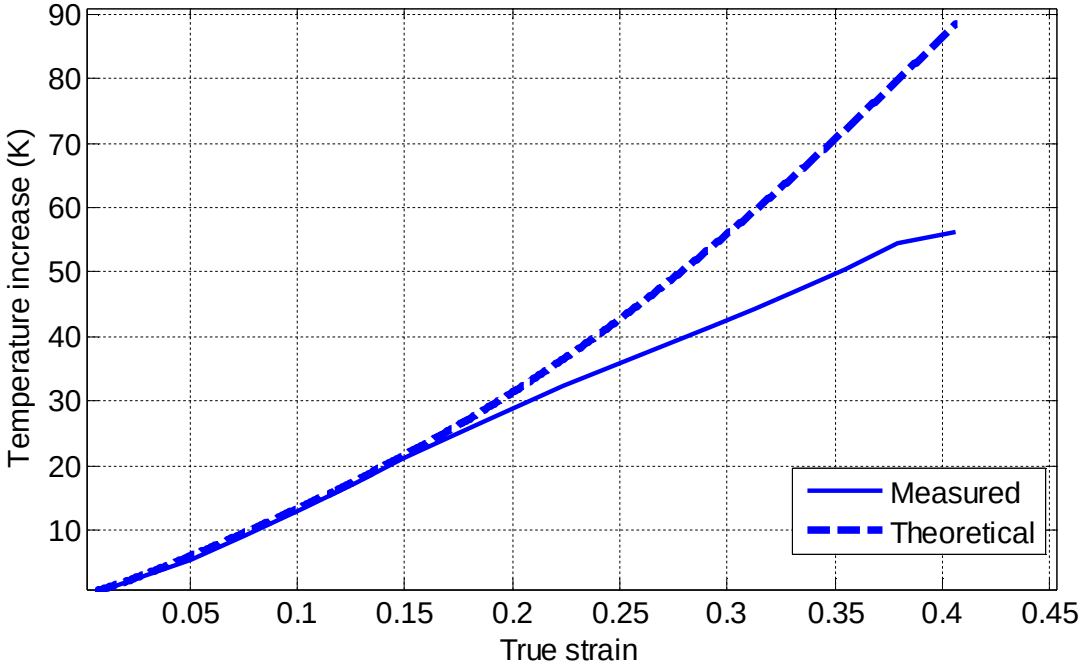

Figure 20. Calculated and measured temperature increase in tests performed at the strain rate of 0.03 $^{-1}$ strain rate.

The calculated temperature clearly overestimates the temperature increase measured by thermocouples during the test. Similar results for both calculated and measured temperatures were obtained by Isakov [1] and Andrade et al. [51]. The reason for this gap between the two curves is most probably the fact that the heating during the applied high strain rate deformation is not fully adiabatic, as there is some heat convection from the specimen to the surrounding environment. Also the mere measurement of the temperature during the test requires heat transfer from the specimen to the thermo-couples. This clearly violates the definition of adiabatic heating, which assumes that no thermal convection and heat transfer occurs. The difference between the measured and calculated temperatures increases with increasing strain rate. The truth is that with the current technology there is no method for measuring the amount of true adiabatic heating during the high rate deformation with very high precision. Finally the mere act of calculating the theoretical temperature increase is not perfectly reliable since equations give only a rough estimate of the temperature.

4.1.1 Continuous heating experiments

As presented above, a widespread consensus in the literature is that the temperature increase during the deformation at high strain rates is responsible for the change in the plastic deformation behavior of stainless steels. Several scientists have studied the effects of the test temperature on material behavior, but to the author`s knowledge there hasn't been any work dedicated to the experimental simulations of temperature increase during high strain rate tests in a low strain rate test, where the deformation without the heating would be practically isothermal.

Figure 21 shows the stress strain curves obtained in the current study. The constant temperature results are similar to the results presented in other publications [59, 60, 55, 43, 61] obtained at various constant temperatures. Increasing the heating rate from 1.4K/min to 2.0K/min only lowers the ultimate tensile strength but doesn't seem to affect the uniform strain significantly. By looking at Figures 17 (a) and 21, the following can be deduced: increasing the temperature during low strain rate deformation (isothermal conditions), will suppress the martensite transformation and lower the ultimate tensile strength of the material. In comparison, increasing the strain rate will have a similar effect on the martensite transformation and ultimate tensile stress since the test conditions will change to non-isothermal where the temperature of the material will increase during the test. Although, it was proposed by De et al. [43]and Rohatgi et al. [14] that the increase in the strain rate has similar effects as a decreasing the test temperature (decrease in SFE) at low strains.

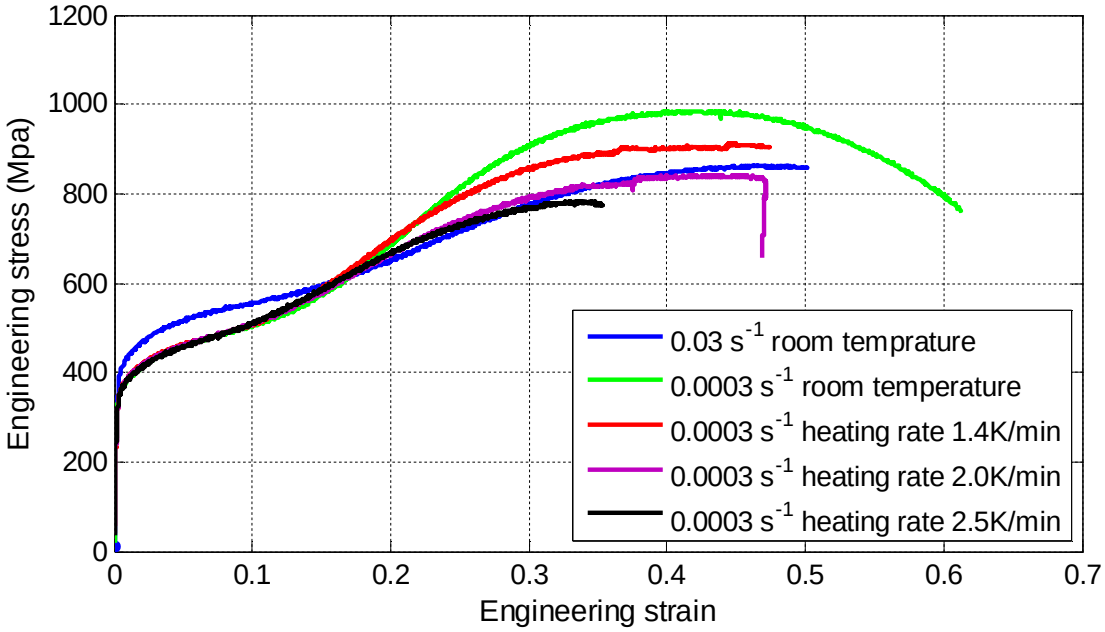

Figure 21. Stress-strain curve for AISI 301L steel at various heating rates.

Up until now the assumption is that adiabatic heating during high strain rate deformation has the strongest effect on the observed behavior of materials, and that the strain rate itself has only a minor effect. To test this theory, the heating rate during the tension test at the strain rate of 0.03 s^{-1} was calculated, and the same heating rate was used in a test at the strain rate of 0.0003 s^{-1}. Figure 22 shows the true stress-strain plots obtained in the continuous heating tests.

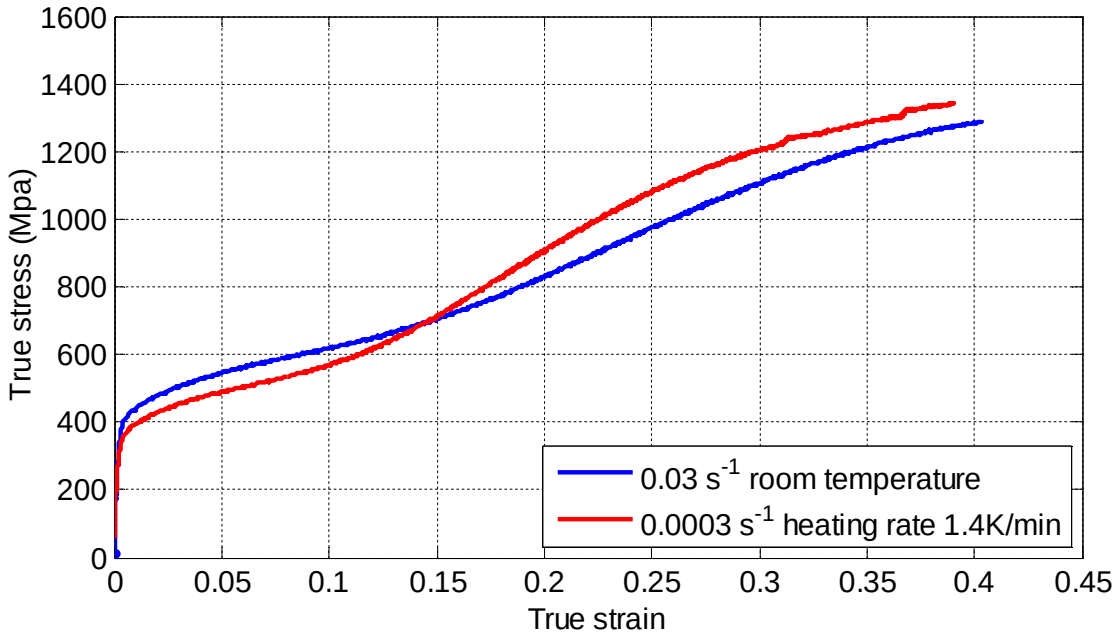

Figure 22. Effect of continuous heating on the true stress-true strain curves at the strain rate of 0.0003 s^{-1}.

Clearly the material`s behavior is not the same; below 15% of strain the flow stress at 0.03 s^{-1} is higher than at 0.0003 s^{-1} with the heating rate of 1.4K/min. However, the relationship between the flow stresses is reversed at strains higher than 15%. The ultimate tensile strength of the specimen deformed at the strain rate of 0.0003 s^{-1} ends up higher than that of the specimen deformed at the strain rate of 0.03 s^{-1}. Since the temperature is essentially the same as a function of strain for both tests, the amount of martensite formed during deformation should be the same as well. Thus, the flow stress obtained at the strain rate of 0.03 s^{-1} should be higher than the flow stress obtained at the strain rate of 0.0003 s^{-1} at strains above 15%. This is clearly not the case and most likely some other factors are affecting the material`s behavior at the strains above 15%.

If the curve obtained at the strain rate of 0.0003 s^{-1} with the continuous heating at the rate of 1.4K/min is compared to the curve obtained at same strain rate without the continuous heating in Figure 17, the flow stress for both show the same behavior below 15% strain. After this point, however, the flow stress of the material obtained at the strain rate of 0.0003 s^{-1} with the heating rate of 1.4K/min is lower compared to the flow stress of the material without the continuous heating. The temperature increase doesn't seem have any noticeable effect on the flow stress below 15% of strain. This is accordance with the fact that the phase transformations mentioned earlier are strongest after 15% strain.

To better understand the effects of the continuous heating, further tests were conducted in order to study the behavior of the material at higher heating rates. The stress-strain plot is divided into two parts, pre and post 15% strain in Figures 23 (a) and (b), respectively.

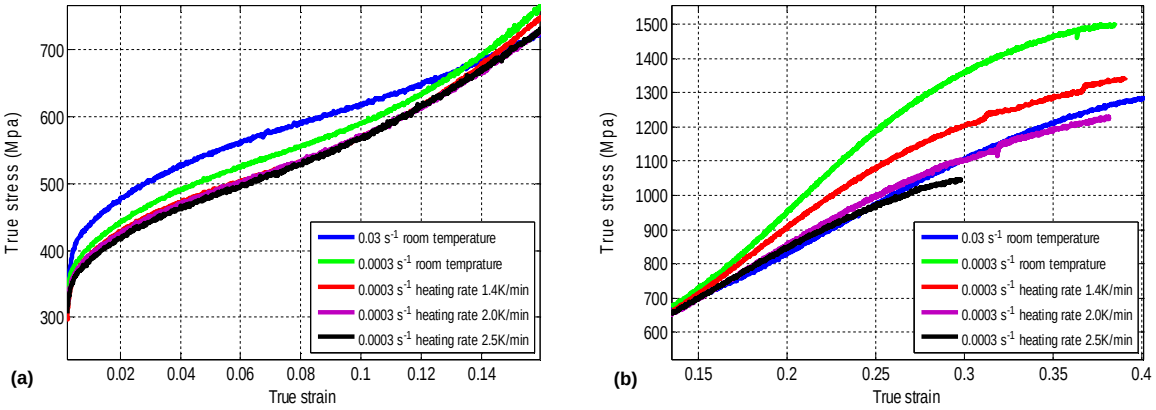

Figure 23. Effect of continuous heating on the true stress - true strain curves at the strain rate of 0.0003 s^{-1} a) below and b) above 15%.

Figure 23 (a) shows that increasing the heating rate does not seem to affect the flow stress in a noticeable way at strains below 15%. All of the curves follow the same path and they all fall below the curve obtained at the strain rate of 0.03 s^{-1}. However, a pronounced change in the material behavior can be seen in Figure 23 (b). The flow stress obtained at the heating rate of 1.4K/min starts to rise as soon as 15% of strain is reached, and increases steadily. The flow stress obtained at the heating rates of 2.0K/min and 2.5K/min start to deviate from the flow stress obtained at 1.4K/min immediately after 15% strain. The flow stress for heating rates of 2.0K/min and 2.5K/min follow the same path until just over 20% strain before deviating from each other. The flow stress obtained at the heating rate of 2.0K/min falls below the flow stress obtained at the strain rate of 0.03 s^{-1} at 35% strain and remains below it until the end is reached. The flow stress obtained at the heating rate of 2.5K/min shows the same behavior, although with earlier start and ending points.

Comparison of Figures 23 (a) and (b) further emphasizes the fact that some other factors besides adiabatic heating must be involved during deformation, and these factors have stronger influence on the material behavior at strains above 15%.

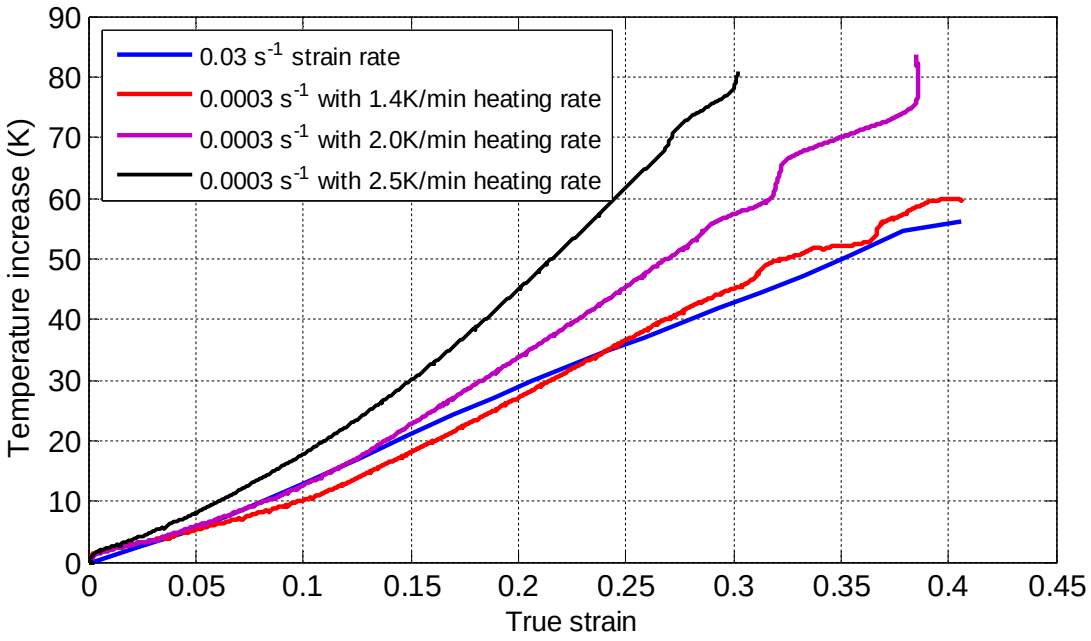

Figure 24. Change in the specimen temperature at different heating rates.

As it can be seen in Figure 24, the temperature for the strain rate of 0.0003 s^{-1} with the heating rate of 1.4K/min drops below the temperature for the strain rate of 0.03 s^{-1} between 5% and 25% strains. The temperature for the strain rate of 0.0003 s^{-1} with the heating rate of 2.0K/min is the same as for the strain rate of 0.03 s^{-1} until 15% strain. After this point the temperature increases at a faster rate, reaching a higher temperature than that measured one at the strain rate of 0.03 s^{-1}.

Finally, the strain hardening rate as a function of strain is shown in Figure 25. For better visibility the results are divided into two parts. Figure 25(a) shows the strain hardening behavior obtained at the strain rate of 0.03 s^{-1} and at the strain rate of 0.0003 s^{-1} with a heating rate of 1.4K/min. Up until stage 1 (5% strain) both show the same behavior, but from this point on, the strain hardening rate obtained at the strain rate of 0.0003 s^{-1} with a heating rate of 1.4K/min increases much faster than that at the strain rate of 0.03 s^{-1}. This will result in a maximum hardening rate that is higher than the one obtained at the strain rate of 0.03 s^{-1} and it is reached at lower strains. It seems that the mechanisms responsible for higher flow stress of 1.4K/min heating rate acts to increase the strain hardening rate as well.

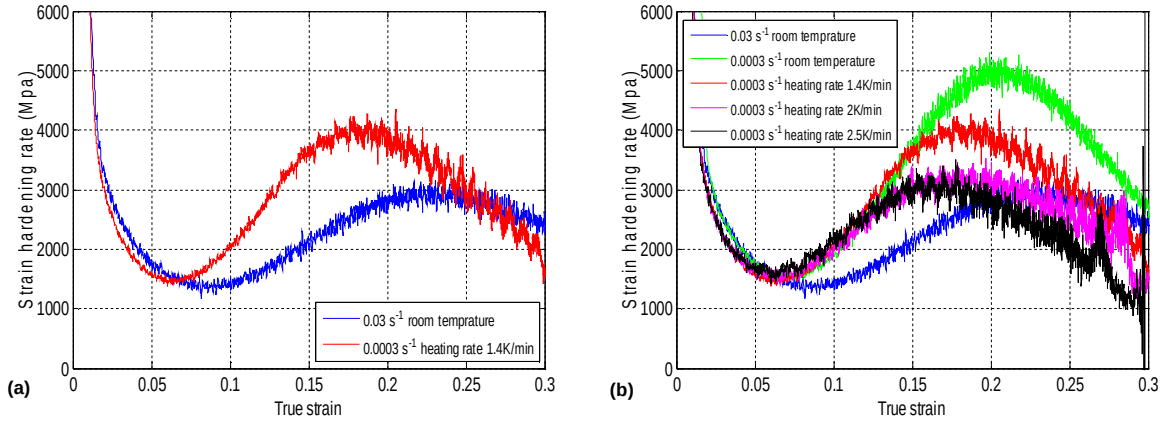

Figure 25. Strain hardening rate as a function of strain at different heating and strain rates.

As shown in Figure 25(b), increasing the heating rate from 1.4K/min to 2.5K/min lowers the maximum value of strain hardening and moves it slightly towards the lower strains but does not seem to affect the strain, at which the strain hardening diverges from the same strain rate at room temperature. This does not come close to replicating the strain hardening behavior obtained at the strain rate of 0.03 s^{-1} at room temperature. The change in the flow stress and strain hardening behavior mentioned above are similar to the results of Noriyuk et al. [59], however the tests were conducted at constant temperatures. This behavior is expected since increasing the temperature will suppress the martensite formation and enhance dynamic recovery.

4.2 Titanium 6Al-4V

This Chapter presents the results for the titanium 6Al-4V alloy. Figure 26 shows the engineering and true stress-strain curves obtained at the strain rates 0.0003 s^{-1} , 0.025 s^{-1} and 1.25 s^{-1}.

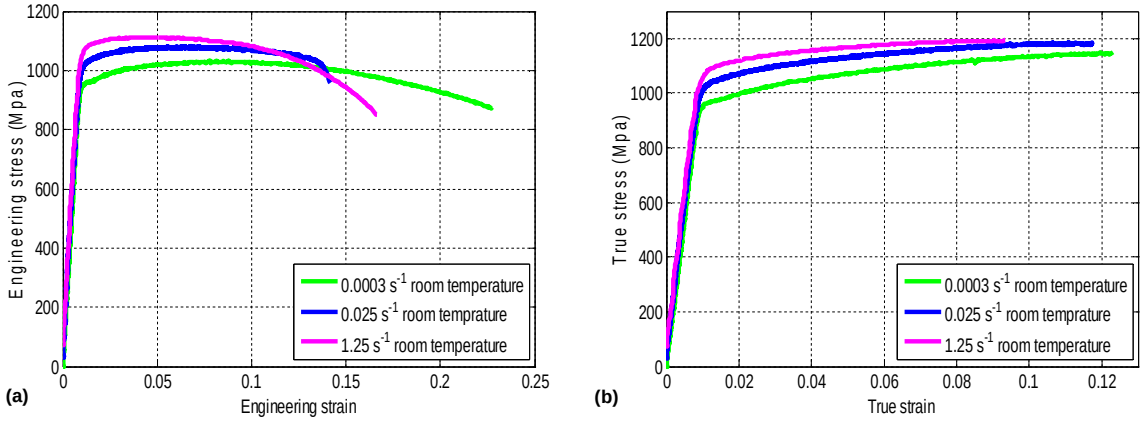

Figure 26. a) Engineering and b) true stress-strain curves for the titanium 6Al-4V at the strain rates of 1.25 s^{-1}, 0.025 s^{-1}, and 0.0003 s^{-1}.

In Figure 26(a), the flow stress obtained for all three strain rates follows the same linear elastic slope until around 1% strain. Plastic deformation initiates at higher strains and stresses as the strain rate is increased from 0.0003 s^{-1} to 1.25 s^{-1}. After the plastic deformation is initiated, the flow stress for these strain rates gradually increases until 10% strain. The strength for the specimen deformed at the strain rate of 0.0003 s^{-1} reaches the maximum point at about 13% strain, decreases steadily and fractures at 23% strain, thus showing the highest ductility. The flow stress at the strain rate of 0.025 s^{-1}, however, shows a sudden decrease at 13% engineering strain. The fracture occurs much earlier for this strain rate, leading to only half of the ductility observed at the strain rate of 0.0003 s^{-1}. For the specimen tested at the strain rate of 1.25 s^{-1}, the ultimate tensile strength is reached at a lower strain compared to the ultimate tensile strength at the two other strain rates. The fracture strain in Figure 26 (a) decreases when strain rate is increased from 0.0003 s^{-1} to 0.025 s^{-1}. However, interestingly, it seems that the increase in strain rate from 0.025 s^{-1} to 1.25 s^{-1} will result in an increase in the fracture strain. The values for uniform strain, however, seem to decrease from about just under 0.1 to 0.05 as the strain rate is increased from 0.0003 s^{-1} to 1.25 s^{-1}, showing that necking is initiated at lower strains with increasing stress. Similar results were also observed in many other studies as well [62, 63, 64, 65].

An increase in the flow stress with increasing strain rate is observed by looking at the true stress - true strain curves obtained at these strain rates (Fig. 26 (b)). As it is expected, increasing the strain rate from 0.0003 s^{-1} to 1.25 s^{-1} increases the flow stress and decreases the strain, at which the ultimate tensile strength is reached. Compared to the stainless steel, the titanium 6Al-4V alloy doesn't seem to show much change in the tensile behavior after the yield point and the curve-crossing phenomenon is absent from the stress-strain plot. This is evidently because there are no phase transformations taking place in this titanium alloy during deformation. The absence of any sudden change in the flow stress in Figure 26 can be better understood by looking at the strain hardening behavior. Figure 27 shows the strain hardening rate as a function of true strain for the stress-strain curves in Figure 26.

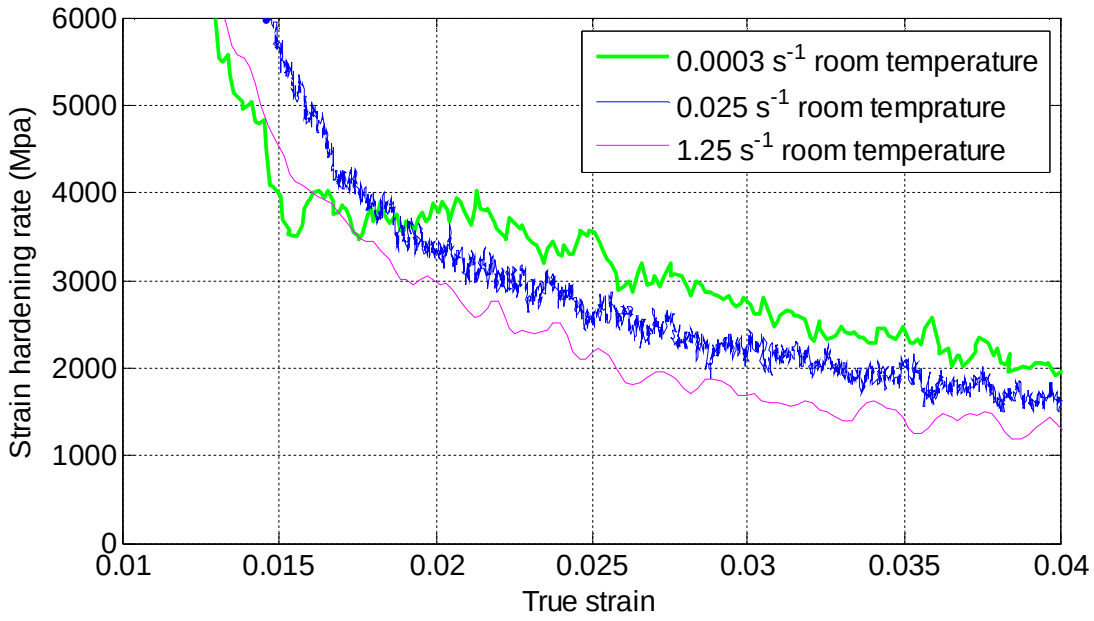

Figure 27. Strain hardening rate as a function of true strain for Ti-6Al 4V alloy at the strain rates of 1.25 s^{-1}, 0.025 $^{s-1}$, and 0.0003 s^{-1}.

Strain hardening behavior for all three strain rates follows the same trend. Strain hardening rate decreases gradually after a sudden decrease at the beginning of plastic deformation. Increasing the strain rate from 0.0003 s^{-1} to 1.25 s^{-1} decreases the strain hardening after 3% strain and the curve obtained at the strain rate of 1.25 s^{-1} shows the lowest strain hardening rate with increasing strain. The overall shapes of the curves obtained here further confirm the lack of any noticeable change in the tensile behavior during deformation.

4.2.1 Continuous heating experiments

The theoretical temperature increase was calculated for the strain rate of 0.025 s^{-1}using Equation (2.5). The obtained heating rate of 10K/min was then applied to the tension test performed at the strain rate of 0.0003 s^{-1}. The heating rate of 4K/min was also used for comparison. The engineering and true stress - strain curves obtained at these heating rates are presented in Figure 28.

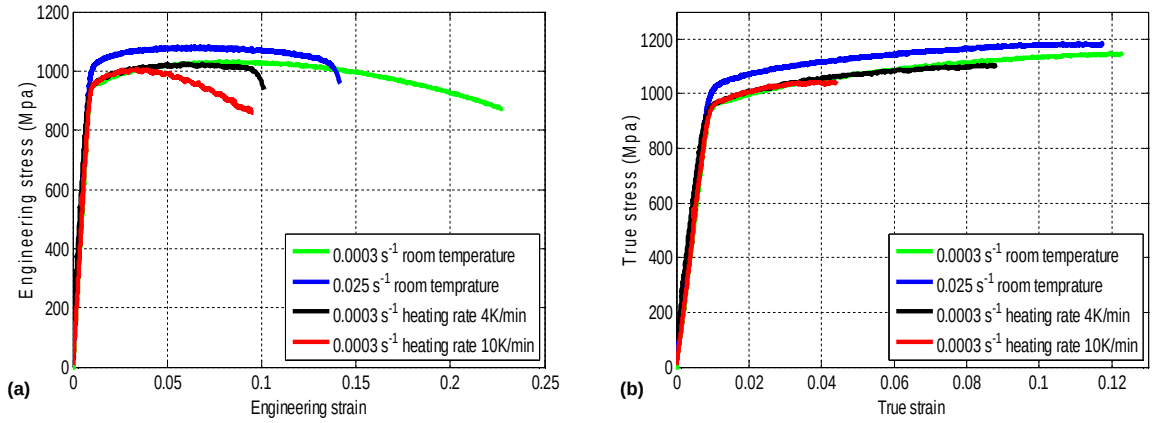

Figure 28. Effect of continuous heating on a) engineering b) true stress-strain curves at the strain rate of 0.0003 s^{-1}.

In Figure 28(a), the shape of the curve obtained at the strain rate of 0.0003 s^{-1} with the heating rate of 4K/min is similar in shape to the curve obtained at the strain rate of 0.025 s^{-1}. However, the flow stress and ductility are lower in the test performed at the strain rate of 0.0003 $^{-1}$ with the heating rate of 4K/min, as the specimen fractures at lower values of strain and stress. Increasing the heating rate from 4K/min to 10K/min does not seem to have any pronounced effect on the shape of the curve obtained at this heating rate before 5% strain. There is a slight increase in the flow stress after the yield point until 5% strain. After this point, the flow stress for the strain rate of 0.0003 s^{-1} with the heating rate of 10K/min decreases at a fast rate leading to the lowest fracture strain. Figure 28(b) shows the true stress - true strain curves obtained at the studied strain rates and heating rates. Applying the heating rate of 4K/min at the strain rate of 0.0003 s^{-1} reduces the flow stress and ultimate tensile strength compared to the strain rate of 0.025 s^{-1}. The increase in the heating rate from 4K/min to 10K/min does not seem to considerably affect the flow stress as it only decreases the uniform strain.

Figure 29 shows the strain hardening behavior of the Ti-6Al-4V alloy as a function of true strain at the studied strain and heating rates. The results are very similar to Figure 27. The strain hardening obtained at all three strain rates more or less follow the same path until 2.5% strain, after which strain hardening obtained at the strain rate of 0.0003 s^{-1} with the heating rate of 10K/min drops drastically. Increasing the heating rate from 4K/min to 10K/min seems to lower the strain hardening at the strain rate of 0.0003 s^{-1} compared to the strain rate of 0.025 s^{-1}. The strain hardening behavior at the strain rate of 0.0003 s^{-1} with the heating rate of 10K/min seems to fluctuate more while decreasing but overall, it stays below the strain hardening obtained at the strain rate of 0.0003 s^{-1} with heating rates of 4K/min and strain rate of 0.025 s^{-1}.

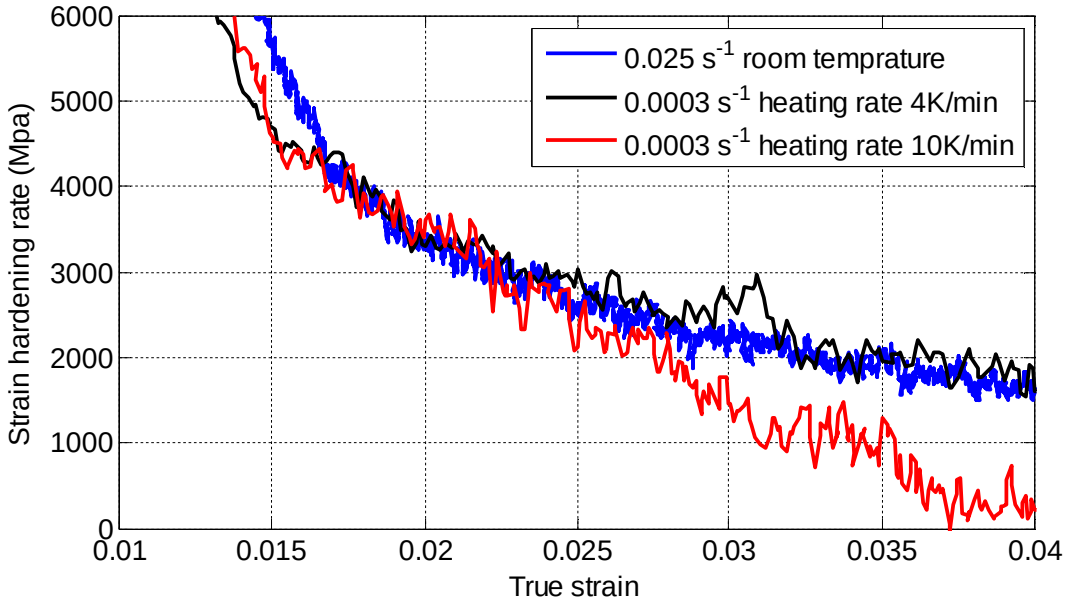

Figure 29. Strain hardening rate as a function of strain at different heating and strain rates.

4.2.2 Fracture profiles

Figure 30 shows the fracture profiles for the specimens used in the tension tests. Figure 30 (a) shows noticeable necking of the specimen tested at the strain rate of 0.0003 s^{-1} at room temperature. The fracture line shows a clear "cup and cone" shape. Thus it can be concluded that deformation at this strain rate is ductile. This is in accordance with Figure 26 (a), where the fracture strain for the flow stress obtained at this strain rate is reached at relatively high strains.

If the fracture area of the specimen tested at the strain rate of 1.25 s^{-1} (Fig. 30 (b)) is closely examined, a slanted fracture line (something between a vertical and a horizontal fracture line) can be seen accompanying slight necking close to the fracture point. It seems that the deformation at this strain rate will result in a shear fracture with slightly ductile behavior. The Fracture area in the specimen tested at the strain rate of 0.025 s^{-1} (Fig. 30 (c)), however, shows very little necking and the fracture line is vertical. The specimen tested at the strain rate of 1.25 s^{-1} is slightly more ductile than the specimen tested at the strain rate of 0.025 s^{-1}. This is a peculiar behavior because increasing the strain rate lead to lowered ductility when the strain rate was increased from 0.0003 s^{-1} to 0.025 s^{-1}. This can be seen in Figure 26 (a) as well: increasing the strain rate from 0.0003 s^{-1} to 0.025 s^{-1} decreases the fracture strain, while increasing the strain rate from the 0.025 s^{-1} to 1.25 $^{s-1}$ increases the fracture strain.

The fracture profile of the specimens tested at the strain rate of 0.0003 $^{-1}$ with heating rates of 4K/min and 10K/min are shown in Figures 30 (d) and 30 (e), respectively. Here the fracture profiles show no necking with vertical fracture lines, and it can be concluded that the material shows brittle behavior at these heating rates at the strain rate of 0.0003 s^{-1}. This is in agreement with Figures 28, in which the strain rate of 0.0003 s^{-1} with heating rates of 4K/min and 10K/min show the lowest fracture strains. Based on these observations it can be concluded that the same drop in ductility for high strain rates can be reproduced by applying the same temperature increase during high strains on low strain rate deformation.

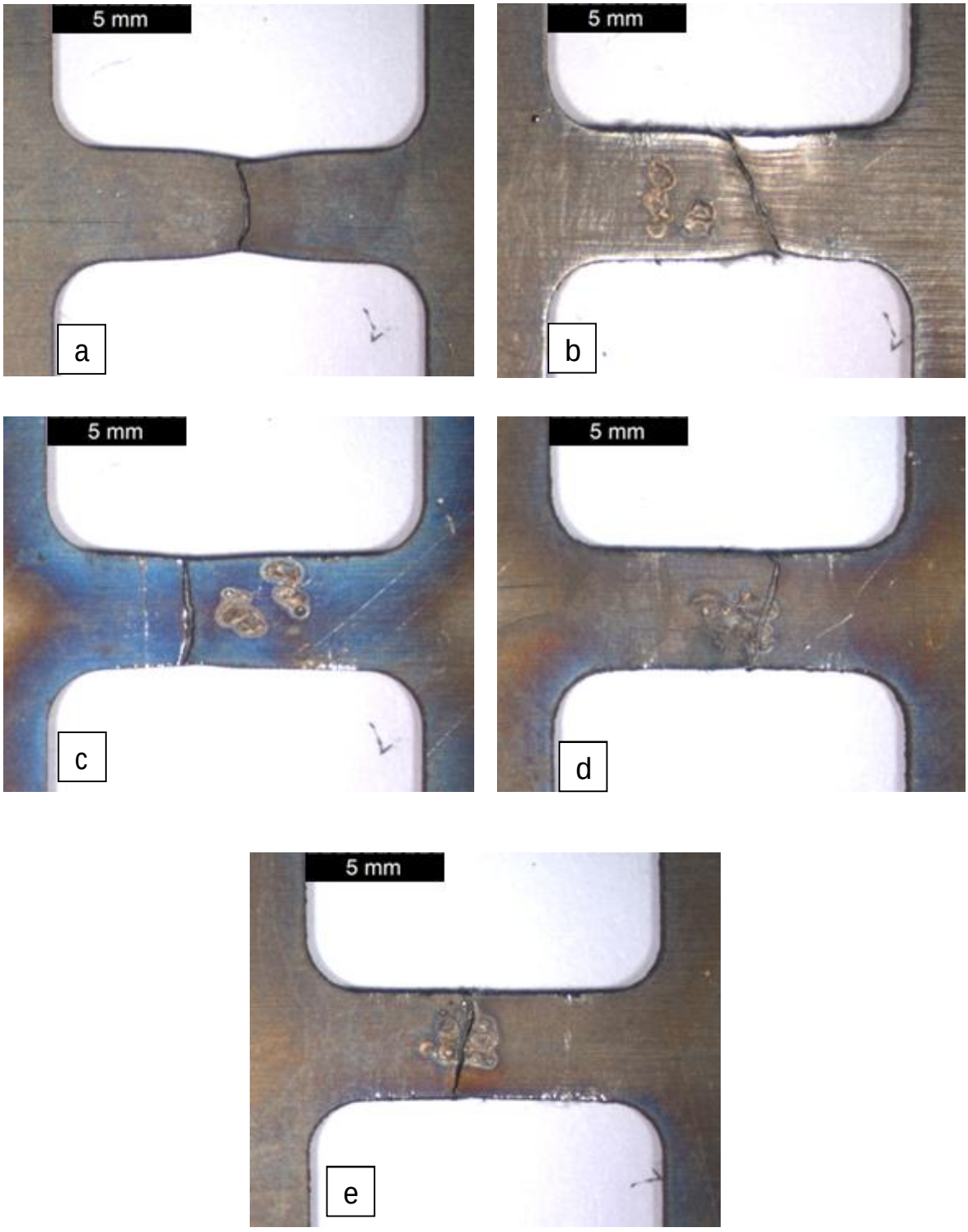

Figure 30. Fracture profiles of the specimens deformed at a) 0.0003 s^{-1} b) 1.25 s^{-1} c) 0.025 s^{-1} d) 0.0003 s^{-1} with heating rate of 4K/min e) 0.0003 s^{-1} with heating rate of 10K/min

5 Conclusions

In this work the tension behavior of metastable austenitic stainless steel EN 1.4318 and titanium Ti-6Al-4V alloy were studied at strain rates between 0.0003 s^{-1} and 1.25 s^{-1}. Also in this work, a new continuous heating experiment for simulating the adiabatic heating was developed. This experiment was designed and used for separating the effects of adiabatic heating from the effects of strain rate. The continuous heating test is performed by measuring and/or calculating the temperature change during adiabatic deformation at higher strain rates and then using the same heating rate in an isothermal tension test at a lower strain rate. This creates essentially identical instantaneous thermal conditions for the tests performed at two significantly different strain rates.

Without the continuous heating, the flow stress of the stainless steel after about 15% of strain at the higher strain rate is lower than the flow stress at a significantly lower strain rate. A part of this behavior can be explained by the adiabatic heating and consequent thermal softening at the higher strain rate. However, this behavior does not change even if the material is deformed at the lower isothermal strain rate and is continuously heated simulating the adiabatic conditions of the higher strain rate. Therefore, in addition to the adiabatic heating, the strain rate itself must play a major role in the strain induced phase transformation. On the other hand, the flow stress of the titanium alloy was higher at higher strain rate compared to the flow stress at the lower (isothermal) strain rate at all strains also when the instantaneous temperature was kept the same for both strain rates. Thus, it can be concluded that unlike stainless steel, titanium behaves as expected with increasing temperature during deformation. Finally the decrease is the ductility of titanium for high strain rate deformation can be reproduced by applying the temperature increase during high strain rate deformation on lower strain rates.

For future works, it is suggested that detailed microstructural studies are carried out for the metastable stainless steel specimens during each stage of deformation. The amount of martensite can then be compared to the amount of austenite at selected strains to fully understand how the strain rate affects the strain induced phase transformation.

Bibliography

[1] M. Isakov, "Strain Rate History Effect in a Metastable Austenitic Stainless Steel," in *Doctoral thesis*, Tampere, 2012.

[2] "Tensile Properties," [Online]. Available: http://www.ndt-ed.org/EducationResources/CommunityCollege/Materials/Mechanical/Tensile.htm. [Accessed 29 3 2013].

[3] j. Hodowany, G. Ravichandran, J. A. Rosakis and P. Rosakis, "Partition of Plastic Work into Heat and Stored Energy In Metals," *Experimental Mechanics ,* vol. 40, no. 2, pp. 113-123, 2000.

[4] ASM Handbook vol 13, corrosion, Ohio: ASM International, 2000.

[5] A. K. Sachdev and J. E. Hunter, "Thermal Effects During Uniaxial Straining of Steels," *Metallurgical Transactions A,* vol. 13, no. 6, pp. 1063-1067, 1982.

[6] ASM Handbook, Mechanical Testing and Evaluation, Ohio: ASM international, 2000.

[7] T. Courtney, Mechanical Behavior of Materials, Waveland Press, 2005.

[8] P. Kettunen and V. Kuokkala, Plastic Deformation and Strain Hardening, 2003.

[9] M. Mayers, Daynamic Behaviour of Materials, New york: John Wiley and Sons, 1994.

[10] J. Venables, "The Martensite Transformation in Stainless Steel," *Philosophical,* vol. 7, no. 73, pp. 35-44, 1962.

[11] C. Rhodes and A. Thompson, "The Composition Dependence of Stacking Fault Energy in Austenitic Stainless Steels," *Metallurgical Transactions A,* vol. 8A, pp. 1901-1906, 1977.

[12] A. Miodownik, *Calphad,* vol. 2, p. 207, 1978.

[13] L. Song, H. Qing-Miao, B. J. and V. Levente, "Stacking Fault Energies of Mn, Co and Nb Alloyed Austenitic Stainless Steels," *Acta Materialia,* vol. 59, pp. 5728-5734, 2011.

[14] A. Rohatgi, K. Vecchio and G. Gray, "The Influence of Stacking Fault Energy on the Mechanical Behavior of Cu and Cu-Al Alloy: Deformation Twinning, Work Hardening, and Dynamic Recovery," *Metallurgical and Materials Transactions,* no. 32A, pp. 135-145, 2001.

[15] L. Vitos, P. Korzhavyi and B. Johansson, "Evidence of Large Magnetostructural Effects in Austenitic Stainless Steels," *Physical Review Letters,* vol. 96, pp. 117-210, 2006.

[16] G. Olson and M. Cohen, "A Mechanism For Strain-induced Nucleation of Martensitic Transformation In Metastable Stainless Steel," *Less Common Metals,* vol. 28, pp. 107-118, 1972.

[17] D. Porter and K. Easterling, Phase Transformations in Metals and Alloys, Oxford: Van Nosrtand Reinhold Company, 1981.

[18] B. Cina, *Acta Metall,* vol. 6, pp. 48-762, 1958.

[19] P. Mangonon and G. Thomas, "The Martensite Phases in 304 Stainless Steel," *Metallurgical Transactions,* pp. 1577-1586, 1970.

[20] G. Olson and M. Cohen, "Kinetics of Strain-Induced Martensitic Nucleation," *Metallurgical Transactions,* vol. A 6A, pp. 791-795, 1975.

[21] J. Brooks, M. Loretto and R. Smallman, "Direct Observations of Martensite Nuclei in Stainless Steel," *Acta Metallurgica,* vol. 27, no. 12, pp. 1829-1847, 1979.

[22] R. Reed, *Acta Metallurgica,* vol. 10, pp. 865-876, 1962.

[23] H. Gomes de Abreua and S. Santana de, *Tavaresc, Mater,* pp. 359-366, 2007.

[24] C. Guntner and R. Reed, "Stress-Induced Martensitic Transformations in 18Cr-8Ni Steel," *Transactions of the Metallurgical Society of AIME,* pp. 1713-1720, 1964.

[25] C. Guntner and R. Reed, "The Effect of Experimental Variables Including the Martensitic Transformation on the Low-Temperature Mechanical Properties of Austenitic Stainless Steels," *ASM Transactions ,* pp. 399-419, 1962.

[26] T. Narutani, "Effect of Deformation-Induced Martensitic Transformation on the Plastic Behavior of Metastable Austenitic Stainless Steel," *Materials Transactions,* pp. 33-45, 1989.

[27] T. Narutani, G. Olson and M. Cohen, "Constitutive Flow Relations for Austenitic Steels During Strain-Induced Martensitic Transformation," *Journal De Physique,* pp. 429-434, 1982.

[28] T. Suzuki, H. Kojima, K. Suzuki, T. Hashimoto and M. Ichihara, "An experimental study of the martensite nucleation and growth in 18/8 stainless steel,," *Acta mettallurgical,* pp. 1151-1162.

[29] W. Lee and C. Lin, "The Morphologies and Characteristics of Impact Induced Martensite in 304L Stainless Steel," *Scripta Materialia,* pp. 777-782, 2000.

[30] N. Gey, B. Petit and M. Humbert, "Electron Backscatter Diffraction Study of ε/α' Martensitic Variants Induced by Plastic Deformation in 304 Stainless Steel," *Metallurgical and Materials Transactions,* pp. 3291-3299, 2005.

[31] F. Lecroisey and A. Pineau, "Martensitic Transformations Induced by Plastic Deformation In the Fe-Ni-Cr-C System," *Metallurgical Transactions 3,* pp. 387-396, 1972.

[32] L. Murr, K. Staudhammer and S. Hecker, "Effects of Strain State and Strain Rate on Deformation-Induced Transformation in 304 Stainless Steel: Part II," *Metallurgical Transactions,* pp. 627-635.

[33] T. Angel, "Formation of Martensite in Austenitic Stainless Steels," *Journal of the Iron and Steel Institute,* pp. 165-174, 1954.

[34] J. Talonen, P. Nenonen, G. Pape and H. Hanninen, "Effect of Strain-Induced Martensite Transformation on Mechanical Properties of Metastable Austenitic Steel," *Metallurgical and Materials Transactions A,* vol. A, no. 36, p. 432, 2005.

[35] S. Hecker, M. Stout, K. Staudhammer and J. Smith, "Effects of Strain State and Strain Rate on Deformation-induced Transformation in 304 Stainless Steel: Part I. Magnetic Measurements and Mechanical Behavior," *Metallurgical Transactions,* pp. 619-626, 1982.

[36] J. Patel and M. Cohen, "Criterion For the Action of Applied Stress In the Martensitic Transformation," *Acta Metallurgica,* pp. 532-538, 1953.

[37] G. Powell, E. Marshall and W. Backofen, "Strain Hardening of Austenitic Stainless Steel," *ASM Transactions ,* pp. 478-498, 1958.

[38] J. Gonzáles, R. Aranda and M. Jonapá, "The Influence of Grain Size on the Kinetics of Strain Induced Martensite in Type 304 Stainless Steel," *Applications of Stainless Steel '92,* pp. 1009-1016, 1992.

[39] S. Varma, J. Kalyanam, L. Murr and V. Srinivas, "Effect of Grain Size on Deformation-Induced Martensite Formation in 304 and 316 Stainless Steels during," *Journal of Materials Science Letters,* pp. 107-111, 1994.

[40] G. Huang, D. Matlock and G. Krauss, "Martensite Formation, Strain Rate Sensitivity, and Deformation Behavior of Type 304 Stainless Steel Sheet," *Metallurgical Transactions,* pp. 1239-1246, 1989.

[41] T. Byun, N. Hashimoto and K. Farrel, "Temperature Dependence of Strain Hardening and Plastic Instability Behaviors in Austenitic Stainless Steels," *Acta Materialia,* pp. 3889-3899, 2004.

[42] X. Fang and W. Dahl, "Strain Sardening and Transformation Mechanism of Deformation-Induced Martensite Transformation in Metastable Austenitic Stainless," *Materials Science and Engineering,* vol. A141, pp. 189-198, 1991.

[43] A. K. De, J. G. Speer, D. K. Matlock, D. C. Murdock, M. C. Mataya and R. J. Comstock, "Deformation-Induced Phase Transformation and Strain Hardening in Type 304 Austenitic Stainless Steel," *Metallurgical and materials transactions A,* vol. 37A, p. 1886, 2006.

[44] G. Sanderson and D. Llewellyn, "Mechanical Properties of Standard Austenitic Stainless Steels in the Temperature Range -196 to +800°C.," *Journal of the Iron and Steel Institute,* pp. 1129-1140, 1969.

[45] Y. Tomota, H. Tokuda, Y. Adachi, M. Wakita, N. Minakawa, A. Moriai and Y. Morii, "Tensile Behavior of TRIP-Aided Multi-Phase Steels Studied by In Situ Neutron Diffraction," *Acta Materialia,* pp. 5737-5745, 2004.

[46] H. Bhadeshia, "TRIP-assisted Steels," *ISIJ International,* pp. 1059-1060, 2002.

[47] J. Guimarães and R. De Angelis, "Hardening by Deformation Induced Phase transformation," *Materials Science and Engineering,* vol. 15, pp. 291-294, 1974.

[48] J. Guimarães and C. Eckstein, "Microstructure-Property Correlation in Martensite-Austenite Mixtures," *Journal of Materials Science,* vol. 15, pp. 3043-3048, 1984.

[49] A. Kundu and P. Chandra Chakraborti, "Effect of Strain Rate on Quasistatic Tensile Flow Behaviour of Solution Annealed 304 Austenitic Stainless Steel at Room Temperature," *Journal of Materials Science,* no. 45, pp. 5482-5489, 2010.

[50] J. Lichtenfeld, M. Mataya and C. Van Tyne, "Effect of Strain Rate on Stress-Strain Behavior of Alloy 309 and 304L Austenitic Stainless Steel," *Metallurgicall and Materials Transactions A,* vol. A, no. 37, p. 161, 2006.

[51] A. A. Campos, F. Teixeira-Dias, U. Krupp, F. Barlat, E. F. Rauch and J. J. Gra´cio, "Effect of Strain Rate, Adiabatic Heating and Phase Transformation Phenomena on the Mechanical Behaviour of Stainless Steel," *Strain: An International Journal for Experimental Mechanics,* vol. 46, pp. 283-297, 2010.

[52] W. Lee and C. Lin, "Impact Properties and Microstructure Evolution of 304L Stainless Steel," *Materials Science and Engineering: A,* vol. 308, no. 2, p. 124–135, 2001.

[53] S. Chiou, W. Cheng and W. Lee, "Strain Rate Effects on the Mechanical Properties of a Fe–Mn–Al alloy Under Dynamic Impact Deformations," *Materials Science and Engineering: A,* vol. 392, p. 156–162, 2005.

[54] Y. Wang, Y. Zhou and Y. Xia, "A Constitutive Description of Tensile Behavior for Brass Over a Wide Range of Strain Rates," *Materials Science and Engineering: A,* vol. 372, p. 186–190, 2004.

[55] E. Isaac Samuel, B. Choudhary and K. Bhanu Sankara Rao, "Influence of Temperature and Strain Rate on Tensile Work Hardening Behaviour of Type 316 LN Austenitic Stainless Steel," *Scripta Materialia,* no. 46, pp. 507-512, 2002.

[56] X. Feaugas, "On the Origin of the Tensile Flow Stress in the Stainless Steel AISI 316L at 300 K: Back Stress and Effective Stress," *Acta Materialia,* vol. 47, no. 13, p. 3617–3632, 1999.

[57] H. Mecking, "Strength of Metals and Alloys (ICSMA5)," *Pergamon Press,* vol. 3, p. 1573, 1979.

[58] S. Nanga, A. Pineau, B. Tanguy, L. Naze and P. Santacreu, "Strain Induced Martensitic Transformation at High Strain Rate in Two Austenitic Stainless Steels," *DYMAT,* p. 1023–1029, 2009.

[59] T. Noriyuki, M. Yoshiki, T. Tomoyuki, S. Yuji, F. Kenzo and U. Rintaro, "Stress-Induced

Martensitic Transformation Behaviors at Various Temperatures and Their TRIP Effects in SUS304 Metastable Austenitic Stainless Steel," *ISIJ International,* vol. 51, pp. 124-129, 2011.

[60] K. Spencer, M. Ve´ron, K. Yu-Zhang and J. Embury, "The Strain Induced Martensite Transformation in Austenitic Stainless Steels Part 1 – Influence of Temperature and Strain," *Materials Science and Technology,* vol. 25, p. 17, 2009.

[61] K. Spencer, J. Embury, K. Conlon, M. Véron and Y. Bréchet, "Strengthening Via the Formation of Strain-Induced Martensite in Stainless Steels," *Materials Science and Engineering,* p. 873–881, 2004.

[62] J. Hammer, "Plastic Deformation and Ductile Fracture of Ti-6Al-4V under various Loading Conditions," *Master thesis,* 2012.

[63] Y. Ravi Shriram, "Experimental Investigation of Plastic Deformation of Ti-6Al-4V under various Loading Conditions," *Master thesis,* 2010.

[64] J. Galán Lópeza, J. Peirs, P. Verleysen and J. Degrieck, "Effect of Small Temperature Variations on the Tensile Behaviour of Ti-6Al-4V," *Procedia Engineering,* vol. 10, pp. 2330-2335, 2011.

[65] S. K. Akhtar, Y. Shaojuan and L. Haowen, "Deformation Induced Anisotropic Responses of Ti–6Al–4V alloy Part II: A Strain Rate and Temperature Dependent Anisotropic Yield Criterion," *International Journal of Plasticity,* vol. 38, pp. 14-26, 2012.